Engineering Responsive, Tunable, and Multifunctional Composites

by

Terry C. Shyu

A dissertation submitted in partial fulfillment
of the requirements for the degree of
Doctor of Philosophy
(Materials Science and Engineering)
in The University of Michigan
2016

Doctoral Committee:

Professor Nicholas A. Kotov, Chair
Professor Sharon C. Glotzer
Associate Professor Peicheng Ku
Associate Professor Max Shtein

To my grandfather

ACKNOWLEDGEMENTS

The first time I spoke to Prof. Nicholas Kotov, he asked me my reasons for pursuing a doctoral degree, and what I wanted out of my experience here. I am not sure whether either of us remembers what my answer was, but the one thing I am certain of is that under his guidance I have gained much more than what I imagined that day. I am very fortunate and grateful for his support, encouragement, and mentorship throughout these years. Likewise, I would like to thank my Ph.D. committee, Prof. Sharon Glotzer, Prof. P. C. Ku, and Prof. Max Shtein, for their valuable contribution, wholehearted support, and the vision that set our project in motion. I would also like to thank especially Prof. Max Shtein, for challenging me to think about our responsibility to contribute to science in however small ways.

I thank all the Folders as collaborators and friends. I hope each of them had enjoyed our work as much as I did. These include Pablo Damasceno, Paul Dodd, Matt Shlian, Aaron Lamoureux, Chi-Wei Chien, and many others who have moved on since we started the Folders group. This work would not have been possible without the support of the National Science Foundation, the I-Corps Program, Rackham Graduate School, the Electron and Microbeam Analysis Laboratory (EMAL) and the Lurie Nanofabrication Facility (LNF).

I am indebted to Prof. James Barber, Prof. John Foster, Dr. Huanan Zhang,

Dr. Bongjun Yeom, Dr. Kyounggun Lee, Dr. Christine Andres, Dr. Jian Zhu, Siu-On Tung, and Joong Hwan Bahng, for their scientific discussions that influenced this work; Dr. Ralph Yang, Dr. Robert Hower, Dr. Pilar Herrera-Fierro, Dr. Nadine Wang, and Dr. Katherine Beach for the mentorship and technical support; Harald, a true engineer in every sense of the word, for his enthusiasm that permeates everything he touches; Yichun, Harish, Steven, Jennifer, Carlos, and Julie, for lending me perspective and food to nourish the body; and Albert, for encouraging me to build substance. Lastly, I am thankful for my family for allowing me the freedom to pursue anything that strikes my fancy and conversations on the meaning of everything.

TABLE OF CONTENTS

LIST OF FIGURES

Figure

ABSTRACT

Engineering Responsive, Tunable, and Multifunctional Composites

by

Terry Shyu

Chair: Prof. Nicholas A. Kotov

In recent years, engineering origami, inspired by paper art, is gaining traction in the study of reconfigurability because of its robustness as a mechanical system. These mechanical systems enable functional properties and can be extended to multiple length scales for a range of applications, including biomedicine, sensing, and smart materials. Here we explore two key strategies to enable new materials designs for responsiveness and tunable properties. The first deals with how we can combine desirable properties onto a single material, and the second deals with how the material is arranged spatially.

In this work, we focus on a layer-by-layer (LBL) assembled composite technique, which provides nanoscale control and mechanically robust composites suitable for reversible responsive systems. In the first part of the work inkjet printing is used produce these composites rapidly and to dictate spatial arrangement. We demonstrate combining LBL with inkjet printing to introduce mechanical motion in a solid

nanocomposite system. Next we show using the same materials system and technique to modulate surface properties by inkjet LBL on nanopillar arrays, and propose its application in breath-activated authentication. The final part of the study focuses on an extension of the origami approach to engineer stretchability in conductive composites. Kirigami, the art of paper cutting, controls the deformation within a composite, which in turn gives us control over the strain-property relationship. The reconfigurability enabled by kirigami can also be used for tunable applications. We show that the combination of bottom-up and top-down patterning of composite materials demonstrates new opportunities in materials engineering, and suggest future directions in the field of engineering origami and kirigami.

CHAPTER I

Introduction

Materials science is the study of how we can expand the currently available material properties in relation to its structure and processing. As part of my PhD work, my projects involved cutting papers and printing Andy Warhol's rendition of Marilyn Monroe, which, at first glance, may seem more like a work in the arts than in materials science. To really explain why these projects were relevant in the context of creating new functional materials, we must first start by describing the idea of paper art as a way to create mechanical systems, its application in various engineering fields, and the intersection between materials and mechanics.

1.1 A Brief History of Engineering Origami

The manipulation of planar sheets into 3D objects dates back to the 1600s. Since the invention of paper around 100 BC in ancient China, [1] which spread to east Asia and to the west via the Silk Road, different cultures have used paper folding for packaging and creative endeavors. The term "origami" (ori, fold; kami, paper) is typically used to describe the art of paper folding because of the rich history associated

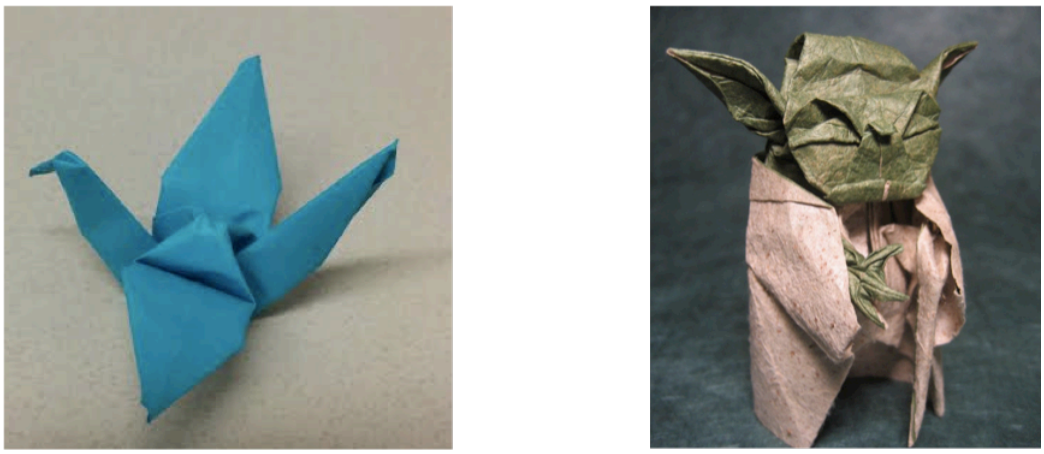

Figure 1.1: The art of paper folding, origami, started from the first description of a paper crane (left, made by the author) and since then evolved into more complicated structures (right, designed by Fumiaki Kawahata, fabricated by Philip West.)

with the popular paper crane, first appearing in a book in 1797 [2] in Japan. The art of origami has since become more and more sophisticated (Figure. 1.1), and mathematical studies have been conceived to describe folding geometry. Origami in its pure form does not allow cutting, whereas its variant "kirigami" involves cutting of the sheet.

Using origami as a technique in science and engineering did not start until the 1970's for its application in deployable structures. In a study in 1969, [3] Miura first proposed a "pseudo-cylindrical concave polyhedral shell" that has a periodic folded pattern. This pattern, as Miura described, was accidentally discovered by mimicking the post-buckling configuration of a cylindrical shell structure, which makes the structure collapsible. The folding pattern is later called the Miura-ori (Fig. 1.2), and has since been used for deployable structures and engineer in-plane stiffness. [4] From its beginning, it can already be seen that origami engineering can be used to couple mechanical behavior and functionality. As a relatively new area of science, origami has seen rapid development in science, engineering, and mathematics in the past few

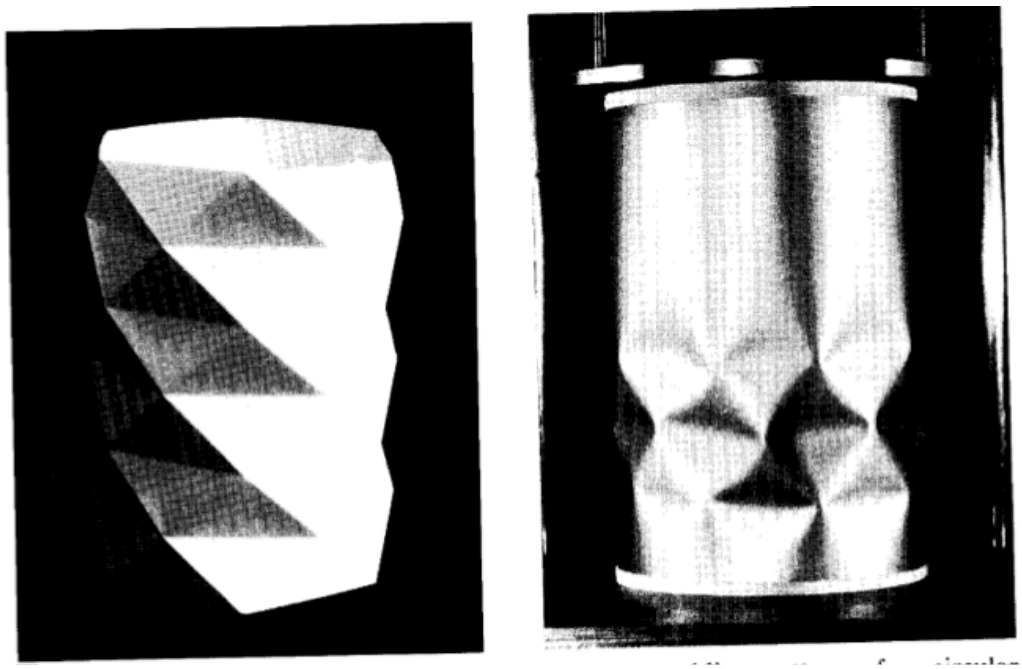

Figure 1.2: The first demonstration of a folding pattern used in the context of engineering, where the folding pattern mimics the natural buckling shape of a cylindrical shell. [3]

decades. The growing interest in origami engineering started in one aspect of engineering as a way to create compact and deployable structures for easy deployment for applications ranging from actuators to space exploration [5, 6]. Another fruitful area of origami engineering is related to the growing interest in creating complex geometries in three dimensions on smaller and smaller length scales. As micro- and nanofabrication become more sophisticated, they are still inherently 2D techniques, and origami provides a way to bring structures into the third dimension. [7, 8, 9] Other emerging aspects of engineering origami also include the underlying physical and mathematical rules for these foldable systems [10, 11, 12] and the nascent 2D starting materials for reconfigurable applications. [13, 14, 15] These emerging areas in origami engineering are discussed in the following sections.

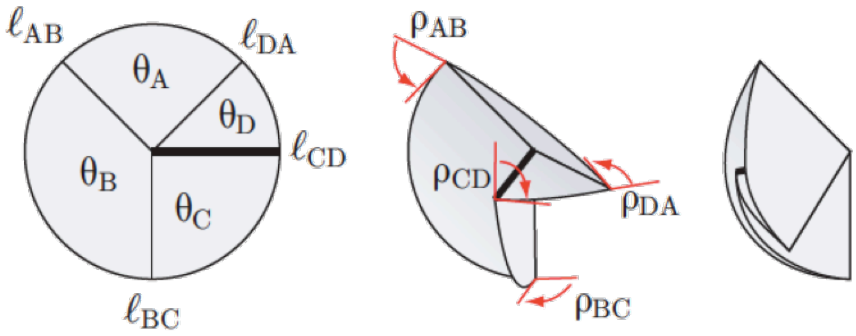

Figure 1.3: The mechanics of the Miura-ori is determined by a small set of folding angles. [16]

1.1.1 Deployability and Foldability

In the context of deployability, the Miura-ori pattern has been studied widely for its intriguing mechanical properties, which are related to the geometry of the folding pattern. The folding pattern consists of two crease lengths that form a repeating parallelogram pattern, a dihedral angle, an acute angle, and an angle that forms once the pattern is folded, which is dependent on the degree of folding. In a 2009 study, [16] Tachi laid out the flat-foldability condition for the Miura-ori pattern. In the simplest form, this condition is dependent on 4 sector angles and 4 folding angles, where one folding angle has to be negative, corresponding to a mountain fold and the remaining three positive, corresponding to valley folds (Fig. 1.3). The crease pattern that satisfies the flat-foldability condition has only one degree of freedom. This property gives rise to Miura-ori's deployability and negative Poisson's ratio.

The kinematics of the Miura-ori pattern dictates that the Poissons ratio is always negative in these patterns across the entire range of actuation as a function of folding angle, or effectively, strain. Treating origami folded structures as rigid panels connected to foldable and frictionless hinges, Demaine, [17] Schenk, [18] Lang,

[19, 20] and others have since studied the foldability for a given structure. The inverse problem can also be solved: based on the desired final origami structure, it is possible to derive the folding pattern. Based on just the kinematics of these folded patterns and ignoring bending of the facets and fatigue at the creases, the deployability depends only on the geometry and is length scale independent. The length scale independence makes a convenient case for metamaterials, where the description of deformation can be translated to any length scale. Silverberg *et al* [21] have exploited the properties of Miura-ori and studied these systems as mechanical metamaterials, focusing on how defects affect the mechanical behavior and guide elastic waves much like in a crystal. As one can expect, however, it was also shown [22] that origami deployability is not controlled by just the kinematics; in real systems thin sheets are also capable of bending deformation, which also leads to mechanical bistability.

The idea of foldability is also relevant in the context of constructing 3 dimensional polyhedra from 2 dimensional nets. Theoretical work by Pendey *et al* [23] points to an algorithmic approach to describe geometric rules that search for an easily foldable path for a given polyhedron. For simple cases like the tetrahedron and the cube, optimal nets are not hard to describe, but the number of possible nets grow very quickly as the the number of faces increases. As it turns out, perhaps unsurprising to origami artists, compactness and short folding pathways are essential considerations in producing high yield polyhedra. This seemingly simple finding is important for experimental demonstrations of self-folding polyhedra that followed.

1.1.2 Toward 3 Dimensionality

As mentioned previously, origami is of interest in creating complex geometries in small dimensions. In the context of creating small structures, since Feynman's "plenty of room at the bottom" challenge in 1959, [24] miniaturization in electronics has come a long way toward their physical limits. The first batch processed micro-electromechanical systems (MEMS) device was produced shortly after. [25] Since then, more complicated mechanical devices such as pressure sensors, actuators, and micromotors have been made, adopting the batch fabrication processes used in silicon integrated circuits. Formation of features relies on specialized etching techniques. [26] These include bulk micromachining, surface micromachining, and the LIGA process (German acronym for lithographie - lithography, galvanoformung - electroplating, and abformung - molding). [27, 28] Most features, however, still lie within the wafer plane.

Microfabrication of electronics is inherently a 2D technology: photolithography is employed, where patterns are optically transferred from a stencil mask to a photosensitive material on a flat silicon wafer. The development of 2D patterning techniques to enable integrated circuit miniaturization has also propelled its expansion into shrinking three-dimensional mechanical structures. However, complex out-of-plane geometries and those that allow for reversible 2D to 3D transformation are hard to achieve using traditional 3D microfabrication techniques such as micromolding, two-photon, and interference lithography. To overcome this limitation, *engineering origami* is particularly attractive as a technique to bring structures into the third dimension. As microfabrication becomes a mature technology, researchers have begun exploring foldable and miniaturized 3D structures to take advantage of existing knowledge in 2D processes while achieving 3-dimensionality. Later in the 1990 and 2000s, the increased research efforts in origami engineering is intertwined with the

rapid development in microfabrication, an intrinsically 2D technology, as a way to create 3D structures using 2D fabrication techniques.

In one early study describing thin film bending, Smela and coworkers [29] showed reversible folding of micrometer scale structures using electrically controlled bilayer actuators. The bilayers made of a conducting polymer polypyrrole and gold undergo reversible bending because of the volumetric change during cation insertion and extraction. Macroscopic bending, folding, and rolling [30] of thin bilayer films have since been used for thin film actuators. It has been suggested that the bilayer conjugated polymer can be used in cell biology because of their suitability in physiological conditions. [31]

Later in 2000, Gracias and coworkers [7] proposed using a lithographically patterned features to form self-assembled electrical networks in 3 dimensions. In this work, only the interconnects were made by photolithography and later glued onto the faces of machine-cut aluminum polyhedra. Here, nothing is actually folding, but it demonstrates an important aspect of origami engineering, where one creates 3D objects out of 2D patterning techniques. It is also around this time, researchers started describing these microfabricated foldable structures as "micro-origami". [8, 32, 33, 34, 35, 36]

Since the 2000's, a flurry of reports have similarly suggested 3D manufacturing by folding [37, 33, 32, 38, 39, 40, 41]. Much like creating a pop-up card, the general strategy is first patterning in-plane, then bring out-of-plane by folding. The key to engineering self-folded structure is through generating a bending moment in a thin film. Hence, miniaturized foldable objects take advantage of 2D patterning techniques while enabling three dimensionality. Some of these strategies include magnetic

forces, surface tension, thin film stresses, etc, and can effectively achieve 3D self-folded structures down to the nanoscale.

One strategy for self-folding takes advantage of length scales. At reduced length scales, surface forces begin to dominate because they scale linearly with characteristic length, while gravitational and elastic forces scale with the length cubed. Taking advantage of the scaling law allows assembly of microscale structures. Py *et al* [42] have demonstrated folding of a liquid droplet by balancing elasticity and capillarity. The capillary force induced radius of curvature L_{EC} is dictated by the following relation, for a given bending rigidity (B) and surface tension (γ):

$$L_{EC} = (B/\gamma)^{1/2}.$$

The Gracias group followed up with several demonstrations of self-folded systems. Leong *et al* [9] have shown self-folding of polyhedra with lithographically patterned soldering material as hinges. First, 2D templates are formed with patterned solder and placed into high boiling point solvent. The molten solder, due to surface tension, draw the nearby faces joined at the hinges, and keep the 3D polyhedra locked in their final folded shape after removing the solvent. Surface tension has proven to work in much smaller length scales for as small as 50 nm cubes. Cho *et al* [43] employed electron-beam lithography to pattern the features, and made hinges from tin, which is melted using plasma etching to heat up and cause grain coalescence. Many recent studies have focused on using these foldable structures for biomedical tools, [44, 45, 46] for their advantages in multifunctionality and manufacturability which can be easily prescribed using self-folding processes.

Folding by thin film stresses has been widely studied, because of its applicability in sub-millimeter scales down to the nanoscale. The key to achieve self-folding utilizing thin film stresses is based on the control of mechanical equilibria. For example, in the case of a bilayer system with the top layer deposited under compression, the system will relax in such a way as to generate opposite internal stresses constrained to each other, and thus creating a bending moment. Stoney [47] and Timoshenko [48] studied stress induced bending in thin metal films to describe the phenomena. The film relaxation is governed by the following relation characterized by the deflection angle θ, which is the length L over the radius of curvature (ρ):

$$\theta = \frac{L}{\rho} = L\frac{6\varepsilon(1+m)^2}{(t_f+t_s)[3(1+m)^2+(1+mn)(m^2+\frac{1}{mn})]}$$

Here, E is the elastic constant, ε is the strain, t the thickness, subscripts f and s indicate film and substrate, respectively, m is $\frac{t_s}{t_f}$, and n is $\frac{E_s}{E_f}$.

From the relation above, one can see that the curvature, and thus the deflection angle, is a function of film thicknesses (t_f and t_s) and the control of strain (ε), which are primarily determined by the deposition process. This relation can also be applied to systems with strains arising from a variety of sources. Thus as thin film processes and deposition techniques play increasingly important roles in multilayer devices, studies in residual stresses during deposition have been critical to avoid delamination and cracking. Later extended to other boundary conditions, carefully constructed bilayers can be used for self-folding applications. Mismatch in lattice spacing, [32] thermal expansion coefficient, [49, 50] and swelling ratios [51, 52] have been used to create stresses in thin films to achieve different degrees of folding, reconfigurability, and in different material systems. Other forms of thin film stress relaxation that

create pattern formation from bending, [53] rolling, [54, 55] and buckling [56] have also opened up possibilities in making periodic or arbitrary micro- and nanostructures.

Shape memory alloys is also a convenient choice to engineer reversibility on millimeter to centimeter scales. [57, 58] The folded and the unfolded states can be achieved by repeatedly annealing and reshaping. Embedding these shape-memory actuators with circuitry to heat up sequentially into a sheet allows one to "program" the final folded shapes. Beyond alloys, Felton *et al* [59] have similarly used resistive joule heating to achieve localized folding with polymer composites that contract above their glass transition temperature.

These folded structures find many applications in biomedicine. Miniaturization of biomedical devices, such as neural probes, [60, 61] is a prime example where going into the third dimension can achieve wide-reaching impact. Besides accuracy, reproducibility, and biocompatibility, biomedical devices must be made small enough to minimize interference with the human body and in batches for medical use. To fabricate high aspect ratio and functional probes, researchers have turned to folded probes. Takeuchi *et al* [62] and Yao *et al* [63] created 3D arrays of microelectrodes from 2D patterning techniques to increase the number of recording sites over a smaller area at around millimeter scales using a magnet and custom jig, respectively.

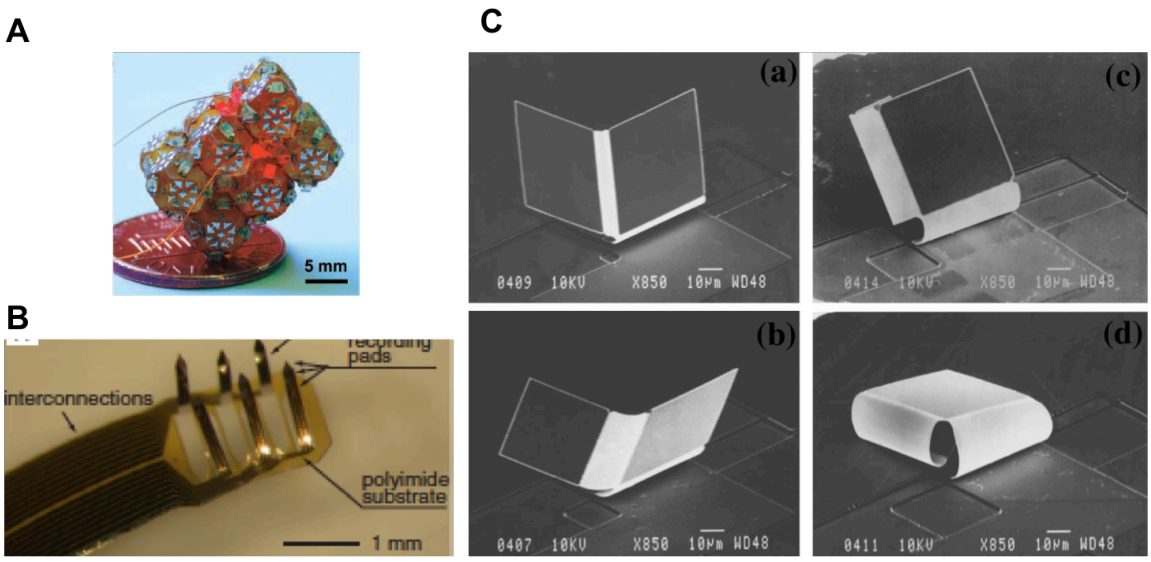

Figure 1.4: Research effort in engineering origami focuses on using 2D patterning technique to generate 3D structures on small length scales. (A) An example of a 3-dimensional circuit; [7] (B) 3D neural probe [62] (C) Folding cube using thin film stresses. [32]

Thus, origami provides a way to access three-dimensional forms from two-dimensional starting materials, where the mechanics can be predictable due to the geometry dependence. In the context of materials science, origami provides a way to design deformation occurring on different length scales. This is fundamental to materials science, where the manipulation of matter on a range of length scales dictate the desired functional properties. By applying engineering origami, we can address the need to engineer responsiveness into materials and dictate functionality.

1.1.3 Self-Assembled Molecular Origami

For many, the first image for the word "origami" in the engineering context is DNA origami. In fact, a great deal of engineering origami in the literature deals with folding of molecular chains. Manipulation of biological matters such as DNA

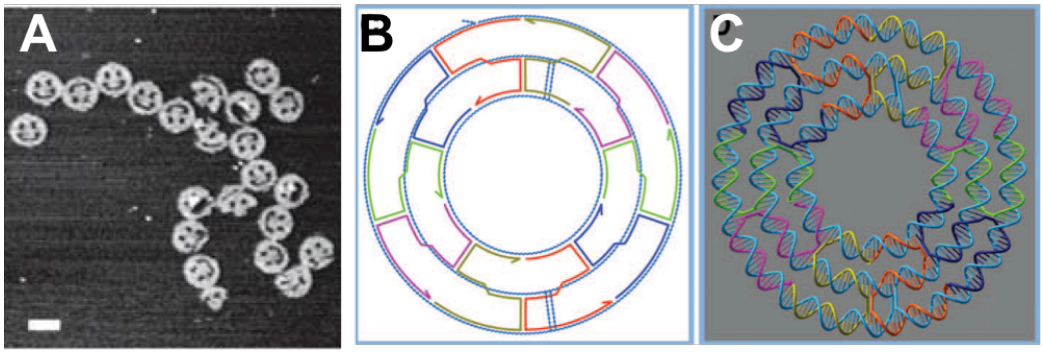

Figure 1.5: DNA origami as a bottom-up nanofabrication technique. (A) Arbitrary shapes formed by DNA self assembly [65] (B, C) Long strand of DNA (blue) folded into concentric circles using short staple strands. [69]

has also gained research attention in the past two decades to create arbitrary shapes in the nanoscale using a bottom-up self-assembling technique, DNA origami. In the molecular world, DNA is an intriguing building block for generating 3 dimensional nanoassemblies.

The double helical structure of DNA and the combinatorially large set of base pairs can be harnessed to design molecular interactions (Fig. 1.5). In 1980s, Seeman conceived the concept of DNA nanotechnology, inspired by the Escher woodcut artwork to create 3D lattice out of linear strands of DNA. [64] By pre-programming the resulting structure, DNA scaffolds are folded into 3D shapes by short staple oligonucleotides. In 2006, Rothemund [65] created arbitrary shapes such as stars, triangles, and lattice patterns with can be created with relatively good yield, using staple strands to hold the long DNA chain in place. The success of this study has thus further spurred the development of DNA origami to create nanocontainers and as a template to arrange nanowires, nanotubes, and nanoparticles in space. [66] Later, it has been shown that gold clusters can be coated with positively charged functional groups and bind to negatively charged DNA. [67, 68] These strategies can be used to manipulate nanomaterials and form arrays and hierarchical assemblies.

Variations of the DNA origami technique have also been proposed to create complex and curved 3D structures. For example, Shih and coworkers [70] have reported using insertion and deletion of base pairs to create twists and curves in DNA origami nanostructures. By controlling the crossovers between neighboring helices, it is also possible to design out-of-plane curvature in DNA origami, [71, 69] further enabling the range of structures that can be made.

1.1.4 Novel 2D Materials

Outside of the context of molecular manipulation, origami by definition implies that the starting materials are typically sheets. Besides deployability and new strategies to manipulate thin sheets, engineering origami and kirigami have also sparked interest in thin, 2D starting materials. Recent attention in novel 2 dimensional materials such as graphene has also been translated to the study of foldable systems.

Back in 1995, Ebbesen and Hiura [13] observed using the atomic force microscope that thin strips of graphite naturally fold in certain angles because of the molecular structure. In particular, the rigid graphite sheet with sp^2 hybridization can form sp^3 character when bending out-of-plane. It had been since proposed manipulating graphitic sheets into desirable shapes using photolithography. With the rise of graphene, the single atomic layer thick allotrope of carbon has been proposed to form 3D structures, much like fullerene and carbon nanotubes, which are considered folded and rolled graphene sheets. Recently Blees *et al* [72] have reported kirigami patterning of graphene. It is expected that a single atomic layer of material should have a low Föppl-von-Kármán number, γ, which measures the ratio between in-plane stiffness and bending stiffness. It is shown that the ripples that form in the graphene sheets

due to thermal fluctuation effectively increases γ by 3 orders of magnitude, close to that of a sheet of paper. The implication is that instead of wrinkling, graphene can be structured, patterned, and manipulated just like in paper art.

These one atomic thin materials such as graphene and molybdenum disulfide become natural candidates to be shaped for applications in engineering origami and kirigami. Using molecular dynamics, Zhu and Li [73] show that hydrogenation of graphene can be used to fold nanocages. Similar to the observation in the graphitic origami, hydrogenation of a carbon atom in graphene induces a structural change from the sp^3 carbon-hydrogen bond. Selective hydrogenation thus creates robust 3 dimensional shapes out of single graphene sheets. This folding scheme is suggested for molecular mass storage and release. As an alternative to graphene, molybdenum disulfide can also be used to for patterning to enhance the ductility and fracture strains. [74] Molecular dynamics calculations show that the more complicated tri-layer structure of MoS_2 is similarly suitable for kirigami patterning.

Despite graphene's remarkable thermal, electrical, optical, and mechanical properties, there remain several challenges in translating the theoretical properties into practical use. Large area graphene sheets are typically grown on metals using chemical vapor deposition and transferred later to the desired substrate. It is well known that the quality is highly inconsistent under nominally identical conditions. Defects such as grain boundaries strongly influence the functional properties of graphene. [75] At the one-atom-thick regime, graphene is strongly influenced by van der Waals forces, and therefore graphene is extremely sticky. [72, 76] The strong adhesion property thus requires the graphene to be suspended or manipulated in solution, and often a workable sample is left to chance. For the many proposed practical applications, reliable methods that yield consistent properties in graphene is much

needed.

On the other hand, graphene-based nanocomposite materials many offer distinct advantages over graphene, considering its relative ease of preparation and tunable properties. Graphene oxide and platelets functionalized by epoxy, hydroxyl, and carbonyl groups allow for stable dispersion in water, making them suitable for processable nanocomposites. [77, 78] Combined with polymer, graphene-based nanocomposite can retain the electrical property above the percolation threshold. The control over thickness and ease of handling also give advantages on using these nanocomposites in practice as the bending stiffness scales with thickness cubed. The load-transfer in polymer and graphene-based nanocomposites can also obviate the brittle fracture observed in monolayer graphene. [79, 80]

1.2 Responsive and Reconfigurable Nanocomposites

So far we have discussed the background in engineering origami and kirigami, and how they are currently used to form responsive and reconfigurable structures. In this study, we aim to investigate how to use the control of mechanics and materials to engineer functionality. We choose layer-by-layer assembled nanocomposite as a system to design responsiveness and reconfigurability. Specifically, nanocomposites present several unique advantages that allow us to achieve desirable properties. Because the interfacial volume between components is drastically increased, greater mechanical reinforcement, electrical conductivity, and other functional properties are resulted. A second advantage is the layer-by-layer assembly can be achieved in the ambient conditions much like in nature. We see that most biological materials, such as bones, diatoms, and seashells, are hierarchical and constructed from the bottom

up, exhibiting a mix of the hybrid and architectured characteristics. [81, 82] As a natural nanocomposite, bones comprise inorganic minerals and organic collagen and demonstrate nanoscale to macroscale hierarchical structure. Their flaw-tolerance and the range of properties achievable with relatively small number of building blocks are often attributed to the sophisticated structural hierarchy. Drawing inspiration from structural hierarchy from the bottom up, it is now possible to design hybrid materials with nanoscale control. Further, the incorporation of zero-dimensional nanoparticles, one-dimensional nanotubes or rods, and two-dimensional nanosheets provide tremendous opportunity for modern materials scientists. The aim of this study is to use these composites for tunable and multifunctional applications by incorporating design of mechanics via origami and kirigami.

1.3 Focus of the Thesis

As we have seen in the previous section, responsive systems are widely studied for metal and polymer systems, and manipulation of folded structures have also been extended to the molecular scale and one-atom-thin materials. Using existing top-down and bottom-up manufacturing methods, we experimentally demonstrate using nanocomposites to engineer tunable, responsive, and multifunctional materials. We also discuss the design of materials and on prescribing functionality. With engineering origami and kirigami, the mechanical behavior of materials is directly tied with the deformation mechanics. Applying these principles, we can control the components and the spatial arrangement of the material, and design responsive materials based on the control of deformation.

1.4 Organization of the Thesis

This thesis is organized as follows:

Introduction and Background. In this chapter, we have discussed the background of engineering origami, how these are relevant in applications across a range of length scales, in optics, MEMS, biomedical engineering, and self-assembly, and the scope of the thesis.

Methods and Techniques. In this chapter, the methods and techniques used in this work are described, including characterization, mechanical analysis, and a discussion on top-down and bottom-up fabrication and patterning techniques.

Responsive Inkjet Printed Layer-by-Layer Assembled Films. In this chapter, we describe a system of layer-by-layer assembled film, which is used to engineer responsiveness. Because of a pseudonegative thermal expansion coefficient that is dependent on the humidity of the surrounding, responsiveness can be used to create motion and used as a visual indicator.

Engineering Properties with Kirigami Nanocomposite. Based on the understanding of strain-dependent conductivity in stretchable conducting nanocomposites, we use a kirigami approach to control materials deformation. With this approach, we can engineer strain-independent conductance over a range of strain, and suggest possible applications.

Tunable Kirigami. Here we experimentally explore using strain-tunable kirigami for modulating plasma properties other potential applications with tunable kirigami.

Summary and Future Directions. In this chapter, we summarize the findings in this thesis, and how they inform future designs of responsive and tunable materials systems. We discuss considerations in time scale, length scale, and the design of deformation.

CHAPTER II

Methods and Techniques

2.1 Introduction

In this chapter, we describe the characterization techniques, and experimental methods relevant to this thesis, including imaging techniques, mechanical analysis, and fabrication techniques. The descriptions of the techniques provided here are not intended to be exhaustive, but should instead serve as a guide for the chapters to follow.

2.2 Microscopy and Imaging

Various microscopy tools are central to the materials characterization in this work, which allows us to gain understanding of a material's structure on a range of length scales. In particular, scanning electron microscopy (SEM) is a commonly used technique for imaging micro- and nanoscale features, with a resolution of down to 1 nm. Analogous to the idea of an optical microscope, a source of illumination in the

form of a high-energy electron beam is focused with a series of lenses onto the sample. The equivalent of a lens for electron beams uses an electric field to deflect magnetic field to focus. Electrons, like a light beam, can be reflected, or backscattered, from the sample. Or, the electron can inelastically interact with electrons in the sample. The ejected electrons are called secondary electrons. Backscatter electrons and secondary electrons are the two primary modes of imaging. The electron beam is scanned line-by-line across the sample under electrostatic and magnetic fields. From the interaction between the electron beam and the sample, the emission of electrons or photons is collected with a detector, allowing us to see the specimen. [83]

Conventional optical microscopy acquires sharp images only at the focal plane. At high magnifications, samples with high level of corrugation, topological features, or non-flat surface result in images that are primarily out-of-focus. Similar to conventional optical microscopy, SEM also does not give 3D details or quantitative analysis. To capture 3D information on a surface, laser confocal microscopy is currently widely used as an optical and non-destructive technique. In 1961, Minsky invented the first confocal microscope, [84] but at the time a sufficient light source did not exist for it to gain much traction. Significant progress in optoelectronics and computer science later on in 1970's through 1990's enabled commercial development of the instrumentation and technology, where it is now widely used in biological specimens.

In laser confocal microscopy, a coherent laser beam is reflected by a dichromatic mirror and scanned over the sample, and the reflected or scattered beam is delivered through a pinhole aperture and into a photomultiplier. [85, 86] The light signal is then reconstructed into an image on a computer. The out-of-focus signals are filtered through a pinhole, and changing the focal plane location results in sequential slices of images that allow for 3D reconstruction of an image that is in focus everywhere. The

advantages of the laser confocal microscopy include minimal to no sample preparation, its non-contact and non-destructive nature, and the possibility to generate 3D slices and quantitative data of sample surface. Furthermore, current technology can use a white light source for true-color imaging, and an LED as a secondary light source to enhance resolution.

2.3 Mechanics

2.3.1 Stress-Strain Behavior

The mechanical property of a material is determined by its stress-strain behavior; one can measure the deformation of the material (strain) by applying a force over an area (stress). For most stiff materials undergoing relatively low tensile stress, the stress-strain relationship is linear through Hooke's law, first stated in 1660, describing the linear relation between force and extension. Thus, stress (σ) is related to strain (ϵ):

$$\sigma = E\epsilon$$

This proportionality constant E is the Young's modulus, which is essentially a material's ability to resist elastic deformation.

Whereas the Hookean behavior describing linear elasticity is easy to characterize and understand, the nonlinear elasticity common in biological, polymeric, and hierarchical materials requires further understanding in the molecular and hierar-

chical structures contributing to the nonlinear response and complex deformation modes. [87, 88, 89] Since the 1940's, studies began to point the elasticity of rubber toward the configurational entropy of stretched polymer chains. The elastic response is dominated by the configurational entropy of the system, where a single elastic chain has many curled-up configurations and only one straight configuration. [90] Hence, stretching a single chain reduces its configurational entropy, and the restoring force comes from increasing this configurational entropy. The strain-hardening, then, is attributed to the fact that the molecular strands cannot be deformed indefinitely.

The deformation of elastic proteins have been widely studied for their wide range of material properties relevant for their functional roles. [91, 92] Many elastic biological materials exhibit a combination of the rubber-like entropic elasticity and strain-hardening effect, where proteins are allowed to unfold during stretching. The energy dissipation that between stretching and re-stretching cycles contributes to the ability for many species to survive in mechanically harsh conditions.

In contrast to biological and polymeric materials, nonlinear elasticity observed in man-made hierarchical materials is due to the different deformation modes or geometric effects. Cellular solids are a particularly interesting class of engineering material that offer desirable strength-to-weight ratio, [93, 94, 95] where the deformation is controlled by linear elasticity, buckling, and collapse. Because of the nonlinearity, the elastic constant of the cellular material here is therefore not well-defined, even though that of the bulk material is well-defined. The condition for buckling is such that the load exceeds the critical buckling load ($P_{critical}$),

$$P_{critical} = \frac{n^2 \pi^2 EI}{h^2}$$

where n is the rotational stiffness of the node where cell walls meet, which is governed by the loading condition, I is the second moment of inertia ($I = \frac{bt^3}{12}$ for a wall of uniform thickness t and width b), and h the wall height. [96]

Given the variety of different stress-strain behavior and the information from which one can derive, it is useful to characterize the deformation response by measuring the stress-strain behavior. This is often done with uniaxial tensile or compressive testing, which yields various material properties by applying a uniaxial force on a specimen until failure. Mechanical properties such as maximum elongation, yield strength, Young's modulus, and more can be obtained.

The tensile test is performed under quasi-static conditions, meaning that the acceleration effect is insignificant on the load measuring devices, and the stress wave propagation is insignificant within the sample. The quasi-static conditions thus differ from sample to sample. Usually a slow enough rate at 0.01 s^{-1} is considered quasi-static; however, to obtain strain rate invariant responses, one can decrease the strain rates by an order of magnitude until further decreases does not change the stress-strain behavior. [97]

2.3.2 Finite Element Modeling

Computer simulation techniques have established their increased practical importance in many complex engineering and physical science problems. It is now possible to simulate interactions of matter from the most fundamental molecular motions and intermolecular interactions, on the scale of molecular dynamics, to interactions much greater than interatomic distances, such as continuum mechanics.

For purpose of our study, we focus on the continuum case. The continuum hypothesis assumes that the characteristic length scale of interest falls within the range where the local density per unit volume is insensitive at the length scale of interest for arbitrary volume V. Here, the continuum description of the system is a coarse-grained, smoothed distribution of continuous densities for mass, momentum, and energy, for systems comprised of a large number of particles, N. [98] This is a good description of the collective behavior of the system, but we should recognize that the assumption breaks down when N is small compared to the length scale of interest.

For mechanical structures with complex deformation and loading scheme, it is useful to analyze deformation using continuum computational techniques, lending us insights to stress concentration, and predict a large number of geometries and parameters. For example, the post-buckling behavior of cellular solids is often analyzed by finite element modeling. [99, 100, 101]

Mechanical structures, regardless of their size and shape, can be broken down into several structural forms, which are composed of smaller units of structural elements. Solving differential equations in a continuum requires discretization and approximation that, in the limit of appropriate discrete elements approach the true continuum solution. Geometry, surfaces, tensile or compressive forces, and three-dimensional materials properties all contribute to the analysis, which is often complicated to solve by hand. This process is automated by numerical methods that approximate the solution. In finite element modeling (FEM), the structure is discretized, or meshed, by dividing the structure into elements and nodes. A set of linear equations are formulated with unknowns at each node, and the linear equations are solved to output stresses, strains, and displacements. Because the inputs

and boundary conditions are the same, the results of a given simulation is the same for an FEM sample every time. The mesh size is decreased until the results do not change with decreasing mesh size.

A number of commercial software packages are available for solving partial differential equations in finite element models. In our study, we used Abaqus-C3D15, a three-dimensional continuum elements code.

2.4 Fabrication Techniques

2.4.1 Thin Films

Thin films are relevant in everyday life in various applications, including optical coatings, semiconductor devices, surface finishes, etc. There are many deposition techniques to form thin films, including various types of physical vapor deposition (PVD) and chemical vapor deposition (CVD) that produce thin metal, polymer, and dielectric layers. These vacuum processes have highly controlled particle density and stoichiometry, with the advantage of high uniformity, smooth coverage, and purity. In contrast with these vacuum processes are ambient deposition techniques that also enable fine control over nanoscale architecture, but have vastly different assembly scheme. Here we focus on the discussion of layer-by-layer assembly (LbL).

LbL has been employed to fabricate a wide variety of nanocomposites that combine seemingly incongruous properties, incorporating aspects of mechanical, electrical, biological, thermal, and optical properties of the constituents. [60, 102, 103,

104, 105, 106, 107] Polyelectrolyte monolayers alternately adsorb, attracted to each other by a number of intermolecular interactions, including: electrostatic, hydrophobic, hydrogen bonding, biological recognition, among others. The adsorption process is repeated with nanometer control over layer structure, thickness, and composition. LbL offers simplicity and versatility compared to other techniques with nanometer control. LbL thin films are also considerably more stable in physiological conditions due to the cooperative effects of multiple interactions among the film components.

In a typical LBL assembly process, glass or silicon substrates are cleaned with piranha solution (3:1 sulfuric acid and 30% hydrogen peroxide). The clean slides are dipped alternatively in oppositely charged polyelectrolyte solutions. These solutions can take the form of polyanion, polycation polymer solutions, or various particle dispersions, allowing for ambient condition assembly and controlled architecture (Figure 2.1). To construct large numbers of bilayers with prescribed dipping time (5 min) followed by rinsing and drying, a NanoStrata robot [108] is used. Other methods to speed up and automate the LBL construction include spin-assisted and spray-assisted LBL. [109, 110]

Vacuum-assisted flocculation (VAF) is an alternative construction method [111, 78, 103] to assemble nanoscale components into nanocomposites, where measured amounts of polymer solution are combined with dispersed nanomaterial, and filtered through with a vacuum filter. Similar to LbL, VAF also produces a layered structure. Different from LbL, however, VAF is a much faster process while sacrificing the level of precise nanoscale control. For example, stretchable nanocomposites have been shown to have superior conductivity when made by LbL compared to VAF. [111]

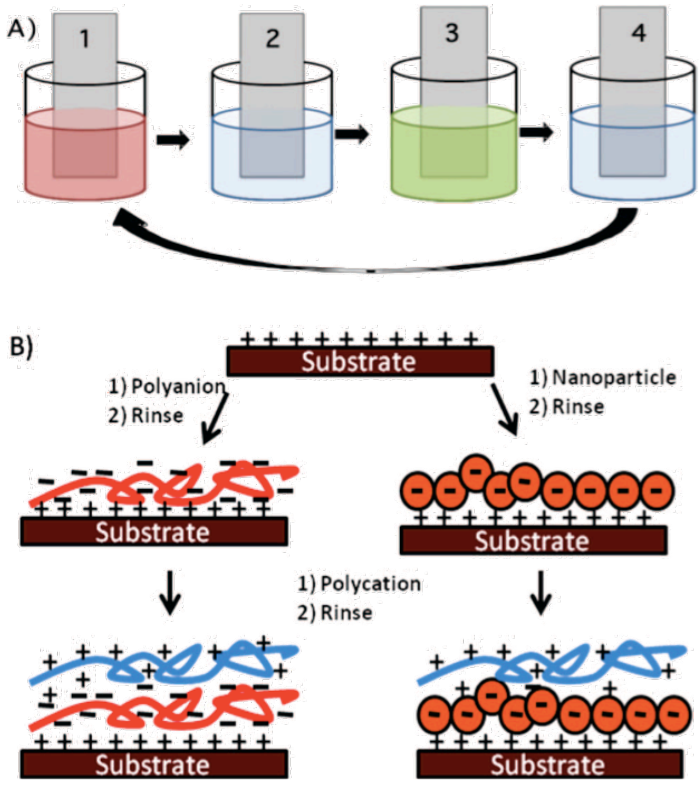

Figure 2.1: Typical LBL assembly process. (A) Clean slides are dipped alternatively in oppositely charged polyelectrolyte solutions, with rinsing and drying steps in between. (B) The clean substrates are positively charged. Monolayer adsorption takes place during each dipping step, here polyanion, polycation, and nanoparticles are incorporated in a layer-by-layer fashion. Adopted from [107]

2.4.2 Photolithography

Photolithography is a technique that writes a CAD pattern onto a stencil mask, which then is transferred onto a planar substrate with a photosensitive resist. In our process, the pattern is designed in L-Edit and written onto a 5" stencil mask plate using the Heidelberg μPG 501. The mask plate with the laser written pattern is developed in MF 319, a developer, then placed in the chrome etch tank to pattern the chrome layer, after which the mask plate is cleaned in a water cascade and is placed in a Nanostrip bath, a commercial version of piranha solution, followed by a second water cascade step to clean the remaining photoresist.

Once the mask plate is patterned, an exposure tool is used to transfer the mask pattern onto the substrate. For example, the GCA AS200 AutoStep, an i-line (365 nm) 5:1 projection tool is used to optically transfer repeated patterns tiled on a single substrate. The substrate used here is typically a 4" wafer with a layer of spin-coated photoresist. Depending on the dimension of the pattern, different thicknesses and type of the photoresist is spun. For best results, the thickness of the resist is on the order of the depth of the pattern. In our process we have used SPR-220 (MicroChem) for thicknesses between 3-8 μm and Shipley 1813 (MicroChem) for thicknesses between 1 to 2 μm.

Thus far, the pattern is transferred from the design to the mask, then onto the photoresist. To transfer the pattern from the photoresist onto the wafer or thin film on a substrate, we use an etching step. For creating free-standing films with the patterning, typically a sacrificial silicon dioxide layer is used. The standard lithographic steps are followed, and in the final step, the SiO_2 layer is dissolved using hydrofluoric acid (HF), while the free-standing film is released. [112] There exists

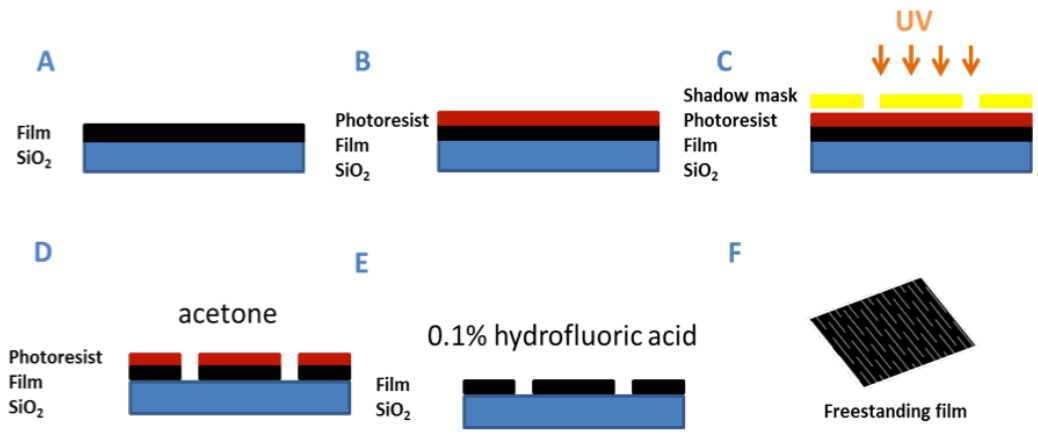

Figure 2.2: Typical lithographic steps. (A) A film is deposited on silicon dioxide glass slide or sacrificial layer. (B) Photoresist is spin-coated. (C) Using a stencil mask, the pattern is transferred onto the photoresist. (D) Photoresist is developed. The film is patterned using plasma etching, and cleaned with acetone. (E) Dilute hydrofluoric acid is used to detach the patterned film to create (F) a free-standing film.

many ways to fabricate SiO_2 layers, each with different deposition characteristics and etch rates. Generally, thermally grown oxides are formed by oxidizing bulk silicon, and chemical vapor deposited oxides are formed by chemical reactions between silicon and vapor and gaseous species. Because HF etches only SiO_2 and not react with bulk silicon, etching sacrificial SiO_2 is commonly used to create mechanical parts in MEMS. And in our process, this gives us an easy route to release patterned thin films.

Dilute or buffered hydrofluoric acid is typically used for removal of silicon dioxide. Alternatively, photolithography process can also be performed on glass slides, and HF can be used to lift off thin films deposited on glass slides. The schematics of the process is shown in Figure 2.2.

2.4.3 Etching

Wet etching is a technique where an etchant in the liquid phase is used to remove material from the wafer. To etch bulk silicon, proper masking is crucial to ensure selective removal of the material in corrosive environments. Wet etching is a chemical process, and in most materials this is isotropic; the exception is single crystal materials where the different crystal orientations have different etch rates due to the difference in surface energy. Chemical etching consists of three steps: first, the reactive species are adsorbed onto the surface, followed by the chemical reaction, and finally the desorption of reaction products. Each step contributes to the etch rate, in addition to temperature and concentration, which affect the overall kinetics.

In a typical process of silicon wet etching, silicon nitride is used as a mask, and 80°C 35% potassium hydroxide (KOH) as an etchant, with an etch rate of around 1 micron per min in the <100> direction. Isopropanol is added to minimize roughness. In wet etching, the selectivity of {100} and {111} planes are about 400:1. Thus wet etching is commonly used for creating anisotropic features, where the {111} plane acts as a natural etch stop. The selectivity have been widely used to create polygonal silicon templates.[113, 114]

In contrast with wet etching, dry etching [115] involves a gas phase etchant in a plasma, containing reactive ions, free electrons, and free radicals. Typically a chamber is evacuated to low pressure, reactive gases introduced, and an electric field is supplied to create and mobilize ion species in a plasma. Etching occurs when the ionized species react with material surface, forming a volatile compound that is carried away by the gas flow. This process removes the material of choice at a rate controlled by the pressure, flow rate, and RF power, and dimensional resolution

controlled by the flux and the masking resist.

2.4.4 Inkjet Printing and Additive Manufacturing

Inkjet printing technology is a versatile deposition technique for the printing industry, and more recently in thin-film electronics and medical applications. Several reviews [116, 117, 118] describe in detail the historical background and future outlook for inkjet printing technologies. Inkjet printing is attractive for a variety of reasons in manufacturing, because it does not require templates and masks to create intricate shapes and can minimize materials waste. The first inkjet printing device was invented by Lord Kelvin in 1858 for recording of telegraph messages using electrostatic forces. The mechanism of droplet formation from a stream jet was then described by Lord Rayleigh. [119] Several studies related to the fluid dynamics of jet breakup followed, relating theoretical understanding in surface tension, electromagnetic forces, and the piezoelectric effect. It was not until 1951 (US Patent 2566,433) that the first inkjet printer was patented using the Rayleigh description of inkjet breakup. Since then, many types of inkjet printing technologies were developed to manipulate droplet deposition. These techniques can either be continuous or drop-on-demand (DOD).

The continuous mode is operated by applying a pressure wave pattern to break up a continuous stream, typically used for high speed printing. DOD inkjet printing [118] is used widely for its precise drop size and spatial control, in addition to other advantages afforded by the inkjet printing technique, including high level of customization and waste minimization. The ink droplets are formed by a voltage applied to a piezoelectric crystal, which generates a pressure pulse that propels picoliter droplets in a reservoir from the nozzle, allowing for precise patterning.

In this work, we use a commercial inkjet printing system (FUJIFILM Dimatix Materials Printer DMP-2831), and piezo-based 16-nozzle jet cartridge, which can be filled with the desirable ink formulation. Some of the important characteristics for the ink formulation include the viscosity, surface tension, evaporation rate, and pH. [120] The viscosity should be maintained between 10-12 cPs, and the printhead can be heated to lower the viscosity of the printing fluid. The surface tension should be between 28-33 dynes/cm, and surfactants and additives can be used to achieve the desirable surface tension range. The evaporation rate is controlled such that the ink does not dry at the nozzle. Solvents can be added to control the evaporation rate. Lastly, the pH is maintained between 4-9 to ensure no corrosion occurs at the printhead.

Besides the rheological properties, the inks should be filtered using a 0.2 μm filter to ensure fluid flow through the nozzle. The rule of thumb is that any particles in the fluid must be 100 times smaller than the diameter of the nozzle. For the commercial 10 picoliter nozzle, this diameter is 21 μm. Hence, most non-agglomerating and well-dispersed nanoparticles are compatible with the inkjet printing technique.

Based on the control of the ink composition, print parameters, and rheological properties, the control of intricate printed structures can be realized, and incorporation of metallic and ceramic components is possible. Recent development in direct-ink writing, [121, 122] for example, demonstrates the potential in emerging area of additive manufacturing. These techniques are convenient tools to dictate the structure and spatial arrangement of material, with tailored mechanical, thermal, and electrical properties.

CHAPTER III

Responsive Inkjet Printed Layer-by-Layer Assembled Films

In this chapter, we use inkjet printing as a patterning technique to create stimuli-responsive LBL nanocomposites. In particular, LBL has important technological significance in creating nanostructures with controlled thickness, morphology, and functionality, and is suitable for modifying surfaces in the context of contact angles. Initially developed for oppositely charged polyelectrolytes, LBL has been shown suitable for a diverse range of nanoscale building blocks, including proteins, nanoparticles, colloids, and dendrimers. In conjunction with inkjet printing, LBL has also been shown a versatile technique to create selectively patterned nanocomposites with customizable architecture that can be used to modify surfaces. [123, 124]

In the first part of the chapter, we discuss a strategy to fabricate a layer-by-layer assembled, solid stimuli-responsive nanocomposite based on relative humidity changes in the environment. Origami, the Japanese art of paper folding, has inspired a body of studies on self-folding and reconfigurable systems, where 2D patterns compatible with traditional 2D patterning techniques are transformed into functional 3D

objects. These self-reconfiguring systems can create structural materials that automatically assume different configurations based on environmental cues. Successful development and implementation of reconfigurable structures with fast throughput, high customization, and precise spatial control will enable applications in dynamic buildings, aerodynamic skin, microfluidics, sensing, and more. On a larger scale, these self-reconfigurable systems may significantly improve efficiency and reduce energy consumption.

Next, we describe a novel approach to use this humidity responsiveness in layer-by-layer assembled films by creating inkjet printed patterns on a substrate with controlled wettability. The difference in wettability as measured by contact angle between the LBL modified, hygroscopic inkjet patterned area and the superhydrophobic, nanopillar decorated areas gives rise the appearance of hidden images when the surface is fogged by human breath. Potentially usable for anti-counterfeit labels and decorative purposes. The humidity responsive materials point to a unique outlook on how we can think about stimuli-responsive systems and their role in technology.

3.1 Inkjet Patterning of Nanocomposites

As previously discussed in the first chapter, foldable structures and stimuli responsiveness are particularly attractive for mechanical motion in sub-millimeter scales and smaller, because manual manipulation of foldable parts becomes less practical and precise folding emphasizes this challenge. Therefore, it is desirable to devise a new paradigm of manufacturing in which the structures self-fold into their functional forms. To create folded 3D structures, several methods have been developed. These include top-down methods such as focused ion beam, molding, [125, 126] and

stereolithography, and bottom-up approaches such as additive manufacturing and self-assembly. [127, 128, 129, 65] Whether it is to make large or small structures fold on their own from an external stimulus, generating a bending moment is crucial to fold out of the plane. Many strategies have been explored and roughly categorized into a few types to create this bending moment: surface tension, [42, 9, 130] shape memory materials, prestressed or swellable polymers, [131, 132, 53, 133, 134] and thin film stresses. [135, 136, 137] However, significant challenges remain to create curved and angled structures, and those that allow large range of motion. Another challenge is that these self-folding structures often require swellable polymers, hydrogels, or molten metals, which inherently do not allow for reversibility. The idea of using nanocomposites has not been widely explored. To generate completely reversible self-folding structures, a different approach must be used. We will discuss how we can use LBL nanocomposites to generate out-of-plane motion using the inherent pseudonegative thermal expansion property found in these LBL systems.

Here we focus on a particular material system of LBL assembled nanocomposites and inkjet patterning. LBL processes are typically water based, and thus compatible with inkjet printing technology without extensive modification. [138, 124] Combined with the LBL process, inkjet printing enables fast assembly of a variety of nanocomposites including proteins, nanoparticles, colloids, and biomaterials. Inkjet printing assisted LBL also presents to advantage of eliminating the intermediate, often time-consuming, rinsing step. Important to note, however, is that this intermediate step in a typical LBL assembly process is important to prevent the formation of aggregates and essential in thermodynamic stability within the multilayers. [123, 139] Thus, in inkjet-assisted LBL, precise amounts and concentrations of material must be delivered, and the viscosity and droplet spreading on the substrate are important parameters to control the resulting multilayers. For this study we specifically focus on

a system based on LBL assembled cationic poly(diallyldimethylammonium chloride) (PDDA) and anionic poly(sodium 4-styrenesulfonate) (PSS) for its thermal response (Fig. 3.1).

Andres *et al* [140] demonstrated the utility of inkjet printing technique to directly pattern responsive hinges required for reconfigurable nanocomposite origami. P3 single-walled carbon nanotube (CNT, 0.25 mg/mL dispersed in water) and cationic polyurethane (PU, Hepce Chem Co., South Korea, Mw 92,000) were used for the LBL assembled nanocomposite, and $(PU/CNT)_{200}$ was constructed using a typical LBL process.

On top of this $(PU/CNT)_{200}$, cationic poly(diallyldimethylammonium chloride) (PDDA) and anionic poly(sodium 4-styrenesulfonate) (PSS, Mw 70 000) were chosen for the as complementary pairs for the inkjet printed layer-by-layer assembly (Fig. 3.2). The inkjet printed polyelectrolytes assemble into complexes and give rise to electrostatically-held swellable multilayer structures that are strongly influenced by the ambient relative humidity. [141, 142, 143] Reversible water absorption and desorption result in reversible volume changes in the polyelectrolyte complexes. [144] LBL films assembled in this manner produce much more mechanically robust structures compared to swellable hydrogel. In addition, these films are often porous in nature, which allows for rapid water transport suitable for fast response time (t in the seconds range for solid thin films).

The thermal properties as characterized by the coefficient of thermal expansion were determined using a thermal mechanical analyzer (TMA, Perkin Elmer) over a temperature range. Between 35 and 75°C, the CTE of $(PDDA/PSS)_{250}$ was determined to be -368 $\pm$ 9 ppm/°C, compared to -6.5 $\pm$ 9 ppm/°C for $(PU/CNT)_{200}$.

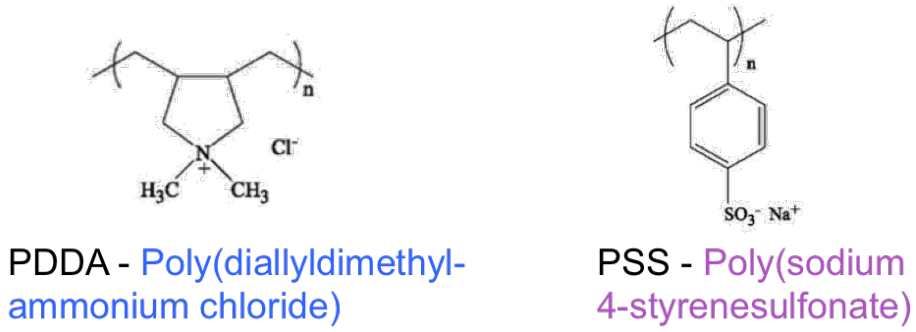

Figure 3.1: The molecular structures of cationic poly(diallyldimethylammonium chloride) (PDDA) and anionic poly(sodium 4-styrenesulfonate) (PSS).

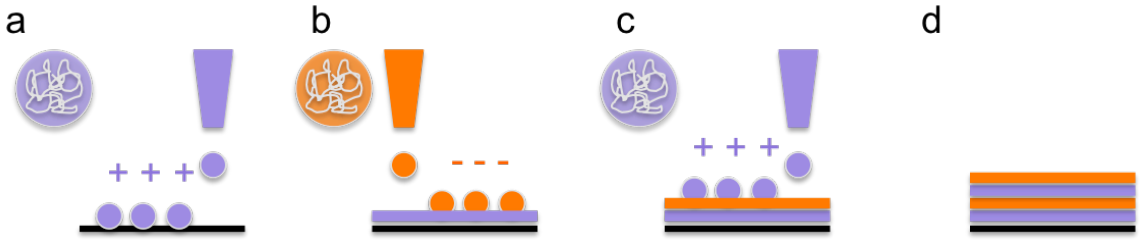

Figure 3.2: Schematic of a an inkjet printing assisted LBL process. (a) Cationic droplets are expelled from the inkjet nozzle, followed by (b) anionic droplets. (c) Sequential alternating complementary cationic and anionic droplets reverse the charges on the surface during each inkjet deposition layer and finally forming an (d) LBL composite.

It was found that the dependence of temperature with the CTE was related to the relative humidity, where the CTE becomes more negative, from -5.3 to -368 ppm/°C as the relative humidity is increased from 0.37% to an ambient humidity of 25%.

We call this humidity-dependent coefficient of thermal expansion (CTE) pseudonegative (PNTE), because of the dependence on water sorption. [145] The PNTE behavior in these LBL assembled films suggests their suitable application in humidity/heat stimuli-responsive systems. As illustrated with the inkjet printed responsive (PDDA/PSS) layers on thin (PU/CNT) strips, heating using an IR lamp is enough to drive humidity out of the system with response time on the order of minutes. The actuated response in deflection angle corresponds well with the earlier Timoshenko equation, given in deflection angle θ:

$$\theta = \frac{L}{\rho} = L\frac{6(a_2 - a_1)(1+m)^2\Delta T}{(t_f + t_s)[3(1+m)^2 + (1+mn)(m^2 + \frac{1}{mn})]}$$

The predicted deflection angle matches well with the experimentally observed values, suggesting that the PNTE contributes to the self-folding of a nanocomposite patterned by inkjet printing.

3.2 Contact Angle and Wettability

Inkjet assisted LBL assembly can also be used as a tool to alter the wettability of a surface. In this section, we describe how we can apply this technique to make a breath-activated stimuli responsive surface.

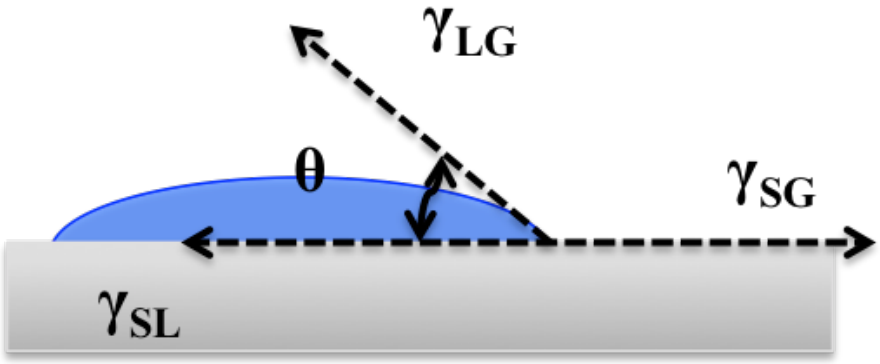

Figure 3.3: Schematic of a droplet residing on a solid surface and energy balance, depicting the interface tensions and the contact angle θ.

Engineered surfaces with different degrees of wettability find important applications such as coatings, aero- and hydrodynamics, and self-cleaning fabrics. At equilibrium, the forces per unit length acting on the line of contact is zero (Fig. 3.3). The angle that the droplet makes at the solid, liquid, and air interfaces is the contact angle, given by the Young's relation:

$$\gamma_{SL} - \gamma_{SG} + \gamma_{LG} cos\theta = 0$$

or commonly expressed as

$$\gamma_{SG} = \gamma_{SL} + \gamma_{LG} cos\theta$$

Thus, wettability is commonly characterized by the contact angle (CA), ranging from 0° - which indicates complete wetting, where liquid spreads on the surface and the surface is known as superhydrophilic - to 180° - which indicates complete non-wetting, where the liquid beads up, and the surface is superhydrophobic.

In practice, textured and hierarchical structures yield good superhydrophobic surfaces. Whereas a fully wetted state called the Wenzel state causes a droplet to cling to a surface, the Cassie-Baxter state yields a composite liquid-air interface on top of the textured surface, in which a droplet tends to roll off easily. [146, 147] This effect can be understood in terms of the apparent contact angle (θ^*), which depends on the contact area between the solid-liquid interface, supported on a composite liquid-air interface due to the surface texture. [148] We can define a dimensionless measure as a design parameter, D^*. Here, $D^* = [(R + D)/R]^2$, where R is the radius of the texture, and D is half the inter-feature spacing, assuming regular surface features. In terms of D^*, the Cassie-Baxter relationship is represented as

$$cos\theta^* = -1 + \frac{1}{D^*}[\frac{\pi}{2\sqrt{3}}(1 + cos\theta)]^2$$

This relationship tells us that at increasing D^*, the actual contact area between the liquid and the solid is decreased, and the apparent contact angle tends toward 180°, which is superhydrophobic. This also implies that to maintain the superhydrophobic property, the surface texture needs to be maintained.

Indeed, because of the dependence of contact angle on surface texture, a critical challenge in engineering surface properties lies in how one can maintain the hierarchical surface features. [149, 150] As we create more hierarchical surface features in decreasing length scales, these small features can be easily damaged during mechanical abrasion, which renders these superhydrophic surfaces impractical. We also note that there are effects of dynamic hydrophobicity, where the contact angle hysteresis and sliding angle are important measures for hydrophobicity in a dynamic case. [151] For the purpose of this study, we will focus on the static case. In the following sec-

tions, we discuss the newly developed PUNO nanopillars as a mechanically robust platform to create a range of hydrophobicity and on top of which to selectively pattern regions of different wetting behavior.

3.2.1 Nanopillar arrays

3D nanoscale surface features can strongly influence adhesion, interfacial interactions, fluid flow, heat transfer, and other phenomena in the macroscale. [152, 153, 154] Numerous examples of 3D nanoscale features that profoundly influence surface properties are found in nature. The lotus effect famously exemplifies the combination of these 3D nanoscale surface features and chemical properties on the leaf surface that contributes to the superhydrophobic and self-cleaning properties. Another example where the sum of all individual nanoscale features contributes to macroscopic effect can be seen in geckos. Gecko's foot hairs, ranging between 200-500 nm, are at the length scale where capillary and van der Waals forces are about comparable. It is thus postulated that while each individual hair contributes only about $10^{-7}N$, millions of these hairs give geckos their famed ability to support their own weight on walls of different hydrophilicities. [155] To artificially create these high aspect ratio features, typically one of several approaches is used, including hydrothermal seed-mediated growth, [156, 157] templated growth, [158, 159] and for periodic patterns, lithography. [160]

In order to increase throughput for large scale fabrication of nanopillars, we have focused on a molding process that uses a master mold created with silicon fabrication technology with deep reactive ion etching. Subsequent polymeric replicas can be made to produce sheets of patterned pillar and hole arrays and compatible

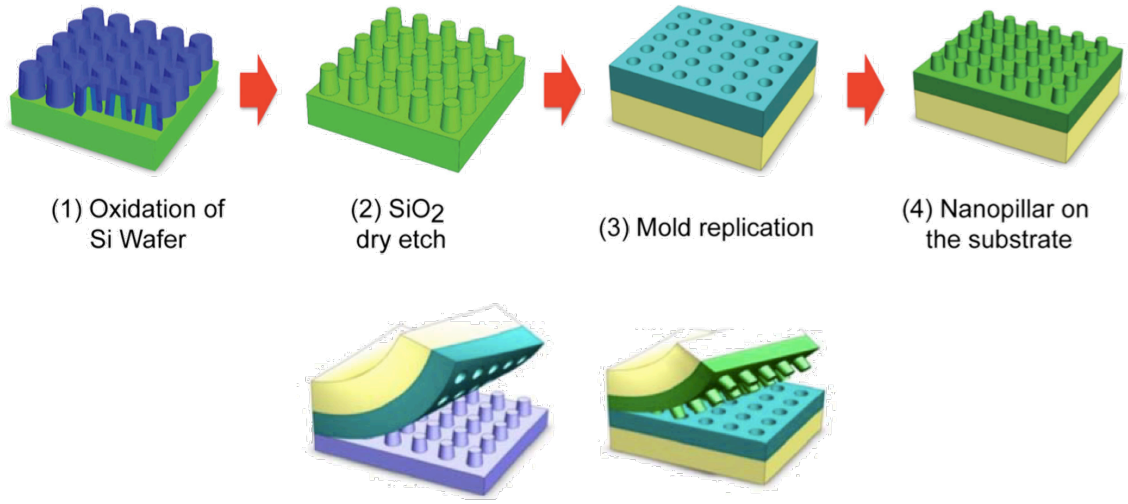

Figure 3.4: Schematic steps to create the nanopillar mold. (1) Thermal oxidation of silicon wafer; (2) dry etching to create desired aspect ratio; (3) once the master mold is obtained, the polymer blend is poured on top to create a negative; (4) alternating positive and negative replications can be created using this process. Bottom depicts the nanohole arrays and nanopillar arrays created by the molding process. [152]

with large scale roll-to-roll processes.

As seen in Fig. 3.4, to create the master molds, silicon wafers are thermally oxidized to have a layer of 500 nm of SiO_2 surface. The surface is patterned by photolithography using a KrF scanner and etched using a mixture of Cl_2, HBr, and O_2 to form the initial master nanopillars. The dimensions and aspect ratios are finetuned by the oxidation time and etching conditions. [152]

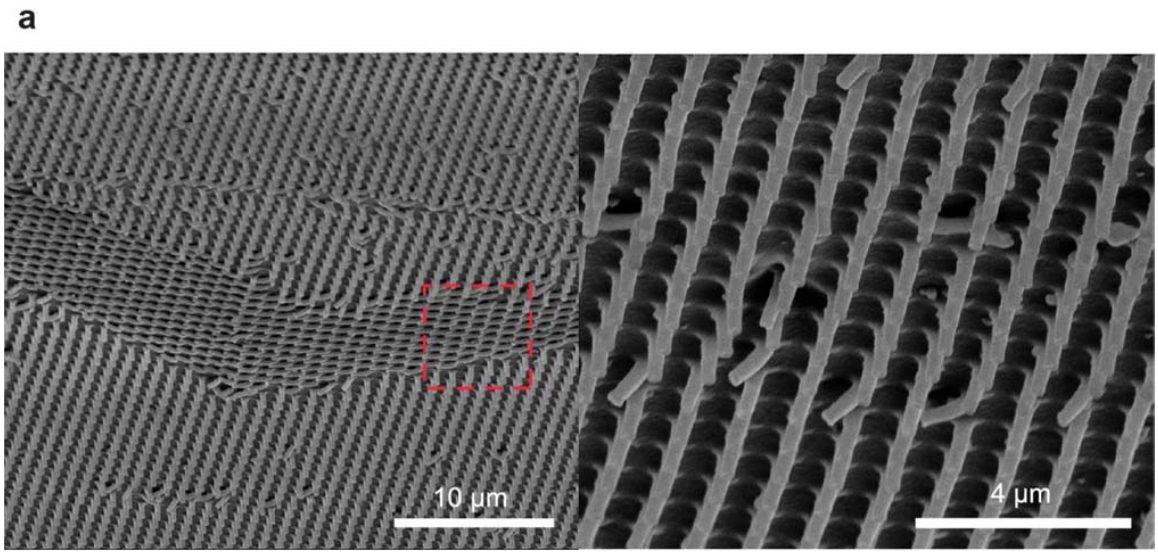

Figure 3.5: SEM images of the nanopillars after 1000 rubbing cycles, showing deformation of pillars but no damage.

To create these nanopillar arrays, the nanomolding process, in practice, requires an optimal balance between the adhesive force and the mechanical strength to create durable nanopillar structures. That is, the adhesive force needs to be high enough to ensure high fidelity of the replicated shape, while soft enough to be deformed and removed from the template, and at the same time mechanically strong enough to remain their shape once the template is removed. This optimal adhesion versus mechanical strength is found in a special blend of polyurethane acrylate (PU) and an adhesive NOA63, denoted as PUNO. This PUNO polymer blend, while undergoing UV curing, shrinks about 1.3%, which allows for detachment from the template (Fig. 3.5). With additional chemical modification, the polymeric high aspect ratio nanopillar surface creates a convenient platform that can support a spectrum of surface wettabilities, ranging from superhydrophobic to superhydrophilic, which is also dependent on the aspect ratio, as controlled by the silicon dioxide doping thickness (Fig. 3.6.a). This level of control will enable responsive smart materials based on the difference in wetting properties.

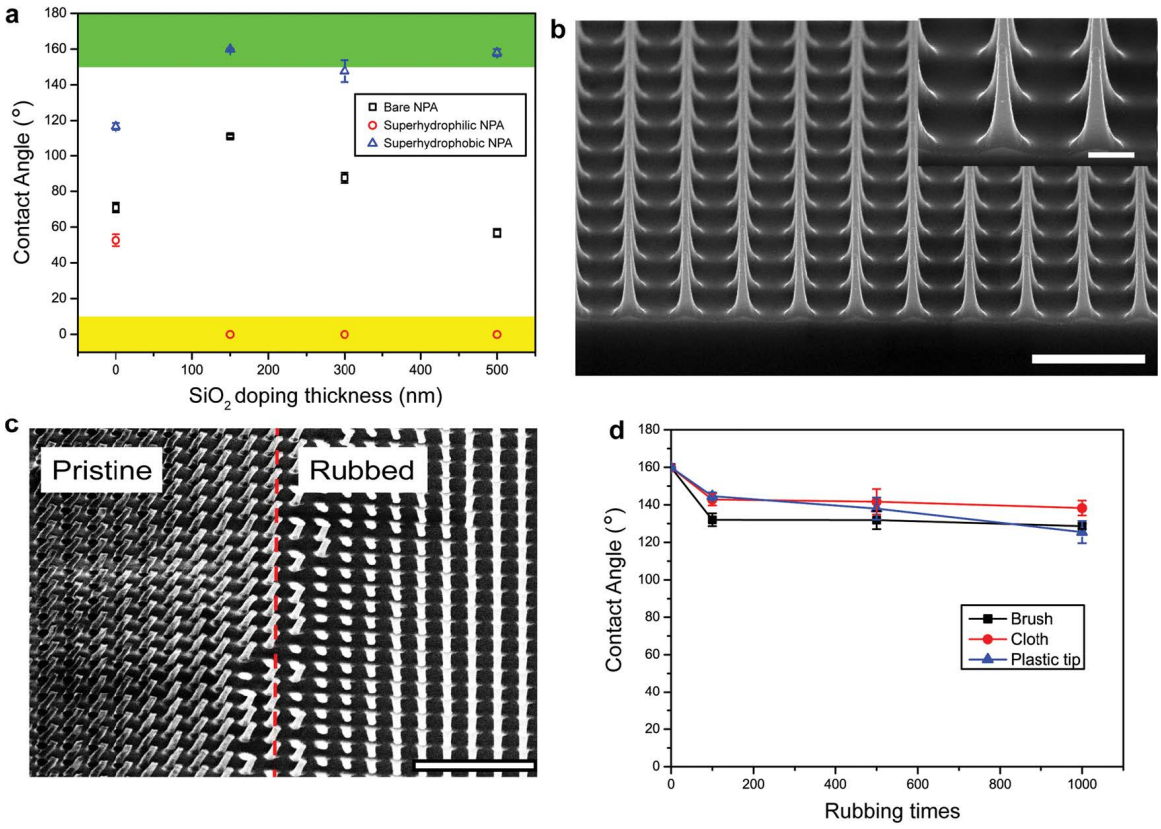

Figure 3.6: Contact angle dependence on surface modification and mechanical abrasion with corresponding SEM images.(a) The contact angle of the nanopillar arrays depends on the thickness of thermally grown silicon dioxide, (b) high-aspect ratio nanopillar arrays, (c) SEM of nanopillar arrays showing clear boundary between the pristine and the rubbed surface, (d) superhydrophobic nanopillar arrays showing stable contact angle over 1000 rubbing cycles.

In nanostructured materials such as the nanopillars used here, the mechanical integrity is crucial to maintain the surface properties during use. It can be seen that nanopillar arrays maintain mechanical integrity after rubbing by bending deformation rather than structural damage. Clear boundaries between rubbed and pristine surface can be seen, but the nanopillars remain on the surface after 1000 rubbing times (Fig. 3.6).

3.2.2 Local Contact Angle Modification Using Inkjet LBL

Contact angle is a common way to determine how well a droplet wets a surface, where low contact angle indicates good adhesion (hydrophilic), and high contact angle indicates poor adhesion (hydrophobic), based on the Young's equation. Site-selective patterning of the contact angles has shown uses for ambient condensation harvesting, microchannels and reactors, heat transfer, and templated thin film growth. [46] Kobaku *et al* [161] have shown using mask or photoresist to pattern sub-millimeter superomniphobic or superomniphilic domains on a highly porous electro-spun surface. Because liquid condensation nucleation rate is strongly dependent on the hydrophilicity, it is possible to tune the nucleation rates using the characteristic contact angle. The condensation property on a given surface can thus be tuned based on the local wetting property. We thus postulate that the ability to direct write a spectrum of hydrophilicities will give us a handle to dynamically control the visual appearance of a surface with patterned hydrophilicities as the relative humidity changes.

The inkjet deposition technique gives the leverage and versatility to create complex shapes with nanometer control over the thickness on microscopic lateral dimensions. Combined with LBL, because the droplets are precisely deposited as

opposed to dip-coated in the conventional LBL assembly, the rinsing step is eliminated and allows for rapid assembly time. Ultimately, we would be able to manufacture high-throughput, ordered nanopillared surface with microscale control over the surface property. Using inkjet LBL, we can selectively alter local contact angle to pattern hydrophilic regions on a hydrophobic surface.

Here, we used a process similar to previously described,[140] using cationic poly(diallyl-dimethylammonium chloride) (PDDA) and anionic poly(sodium 4-styrene-sulfonate) (PSS, Mw 70 000) as complementary pairs for the layer-by-layer assembly. High molecular weight PDDA and PSS were diluted to 0.0025 wt% in deionized water as the positive and negative polyelectrolytes, respectively, and filtered through 0.22 μm filters. The patterns were printed using Fujifilm-Dimatix inkjet printer and alternating cartridges (10 pL drop volume) containing the solutions of PDDA and PSS. Jetting conditions were optimized by adjusting the drive voltage-time waveform for the piezoelectric print-head to produce stable drops. Four bilayers of ink were printed and dried at 35°C in between prints for 2 min on the printer plate, followed by drying on a hotplate for 1 h after the printing steps.

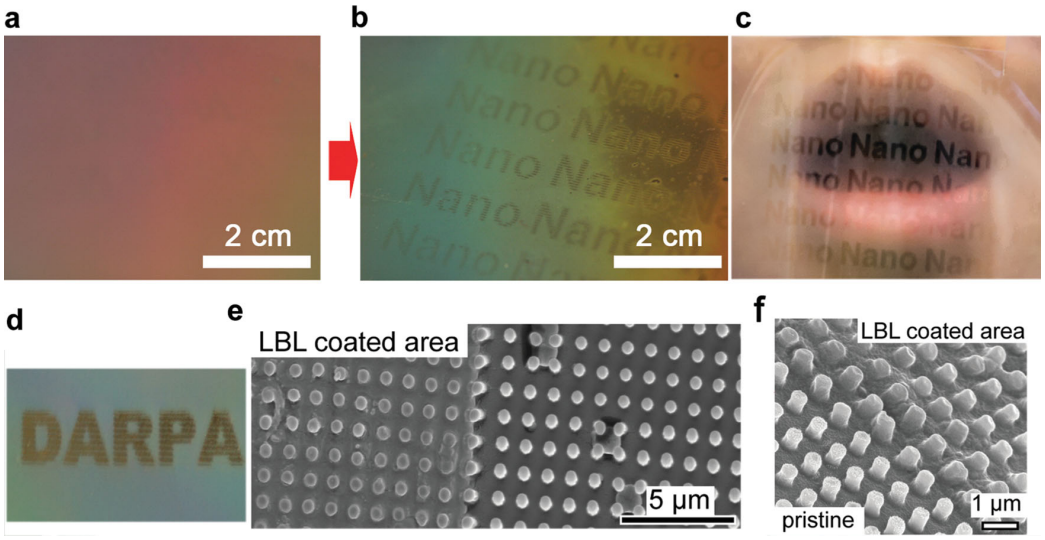

Figure 3.7: Overt and covert images printed on nanopillar arrays using inkjet LBL deposition. Photographs of the nanopillars with hidden images (a) before and (b,c) after exposed to breathing. (d) an overt image printed on nanopillar arrays. (e,f) SEM images showing differences between areas modified by LBL and pristine nanopillars.

3.3 Overt and Covert Images

After inkjet modification of the surface, it is possible to create overt and covert images by the dynamic control of the visual appearance of the nanopillar surface (Fig. 3.7). Depending on the number of layers deposited, either overt or cover images can be created. At less than 3 deposited PDDA and PSS bilayers, the nanoscale coating on the nanopillars does not alter the visual appearance of the film significantly. But because of the changes in wettability between the patterned and non-patterned areas, the few bilayers of the hygroscopic pattern is enough to tune the local contact angle, such that when the printed invisible pattern is exposed to relative humidity change, the images become visible.

With increasing number of bilayers, on the other hand, the spacing between nanopillars becomes filled, creating contrast between the printed pattern and the

pristine nanopillar region. At 5 bilayer and above, the printed pattern becomes visible to the naked eye without having to fog the surface.

Thus, we have demonstrated using transparent LBL coating to modify a nanostructured, superhydrophobic surface, which can be used for anti-counterfeit labeling and authentication. Future studies on the formation of patterns on nanopillar surfaces will pave way toward manipulation of nanoscale surface effects.

3.4 Conclusion

In this chapter, we first surveyed the strategies to create stimuli-responsive systems, focusing on shape-morphing systems inspired by the art of origami. The LBL inkjet printing technique is employed to create hydrated polyelectrolyte multilayers capable of shape transformation on top of a solid nanocomposite, in response to temperature and humidity changes. The reversibility indicates negligible structural changes within the nanocomposite during the shape transformation and robustness of the inkjet printed LBL technique. Possible future direction includes incorporation of plasmonic nanomaterials that have spectral selectivity to responsiveness. The patternability and responsiveness pave way to a range of smart material design.

With the same humidity responsive hydrated polyelectrolyte multilayers, we have also demonstrated a novel application for the stimuli-responsiveness. Based on the idea of selectively modifying surface wetting property, inkjet patterned polyelectrolyte multilayers combined with nanostructural features such as nanopillar arrays can be used to pattern hidden images that are revealed using human breath. Using the inkjet patterning technique, we are able to dictate the spatial arrangement of

materials on a selectively. With control of the nanoscale components and features, we can engineer materials that respond to environmental cues.

Future studies in these materials systems may involve investigating the adhesion between the inkjet deposition and the substrate material. Further, the interaction between the molecular chains of PDDA and PSS and the water can be further fine-tuned for the level of responsiveness. It is also worth considering the structural changes within the LBL multilayers during water sorption and desorption.

CHAPTER IV

Engineering Properties with Kirigami Nanocomposite

By designing the deformation of materials, simple mechanical movements and bistability can be used to couple the deformation mechanics to the functional properties of materials. [82, 153, 134] This coupling effect can give rise to possibility in metamaterials on every length scale. [21, 22] In this chapter, we explore how we can design the deformation of materials by using simple cutting patterns, borrowing the concept from the art of paper cutting known in different cultures as *jianzhi*, *kirigami*, *monkiri*, or *silhouette*. We use the term *kirigami* because of the greater emphasis of this Japanese technique on repetitive patterns and their effects on three-dimensional deformations of paper sheets. We highlight in this work, that the design of deformation based on the kirigami patterning technique can have wide-reaching impact. Here we show the control of strain-conductivity relationship, eliminating the unpredictable strain effects in nanocomposites by controlling the deformation. We will also explore some potential applications related to the reconfigurability in the following chapter.

4.1 Background

Strain engineering has become increasingly important for the next generation of nanocomposites, enabling the combination of mechanical and electrical properties typically unattainable in traditional metals, ceramic, and polymers. [111, 162] There is a great need to further expand the range of accessible strain states and develop new ways to deterministically control strain-property relationships in these systems. [163, 164, 165] The development of multifunctional elastic nanocomposites requires the control of deformation and failure mechanisms in order to retain functional properties under high strains. It is known that stress failure of stiff and brittle materials strongly depends on stochastically-distributed nanoscale and microscale defects, which serve as stress concentrators that promote propagation of microcracks, leading to failure. Many natural and man-made nanocomposites, combining hard and soft components can arrest the propagation of microcracks but their ultimate strains do not exceed 5% at high loading of the stiff components. [166, 167] On the other hand, the stress concentration can be avoided in highly elastic nanocomposites and one can reach strains as high as 470% but some of the functional properties, e.g. conductivity, has to be sacrificed. [111, 162] Interfacial stiffening of polymers chains at the interface with nanoscale components severely limits macroscale elasticity of composites and their ability to relax local strain singularities. Accounting for strain-induced restructuring in several interdependent components adds to the complexity of the multiscale deformations in nanocomposites, and makes predictive modeling of their tensile behavior an arduous task.

In this work we investigate a possibility to increase strain capabilities of highly conductive but stiff materials, borrowing the concept from kirigami. The kirigami technique has recently been used to engineer reversibly deformable two-dimensional

(2D) and three-dimensional (3D) structures, in which patterns of periodic cuts give rise to emergent mechanical behavior. [72, 11, 21] We show that even simple kirigami patterns can offer unprecedented control over stretchability, with only negligible impact on conductance. From this framework, we demonstrate the possibility of making a smart material from the combination of stretchability and conductivity using kirigami nanocomposites.

4.2 The Kirigami Approach

In this work we show that in traditional kirigami, highly periodic cut patterns are introduced into paper sheets to attain desirable topology upon folding. Using standard top-down technique such as photolithography (Fig. 4.1 a), we can extend the technique to micro- or potentially nano-scale. This fabrication process offers scalability and accuracy, providing us the possibility to produce similar patterns across multiple length scales. Here the homogeneity of material must be commensurate with the length scale of the kirigami cuts, which is true for many nanocomposites exemplified by grapheme oxide multilayers made by vacuum assisted filtration (VAF) or layer-by-layer assembly (LBL) techniques (Fig. 4.1 b). [78] By measuring the stress-strain response and comparing it to finite element calculations, we show that mechanical deformation introduced by kirigami patterning may be used to engineer elasticity and multi-functionality.

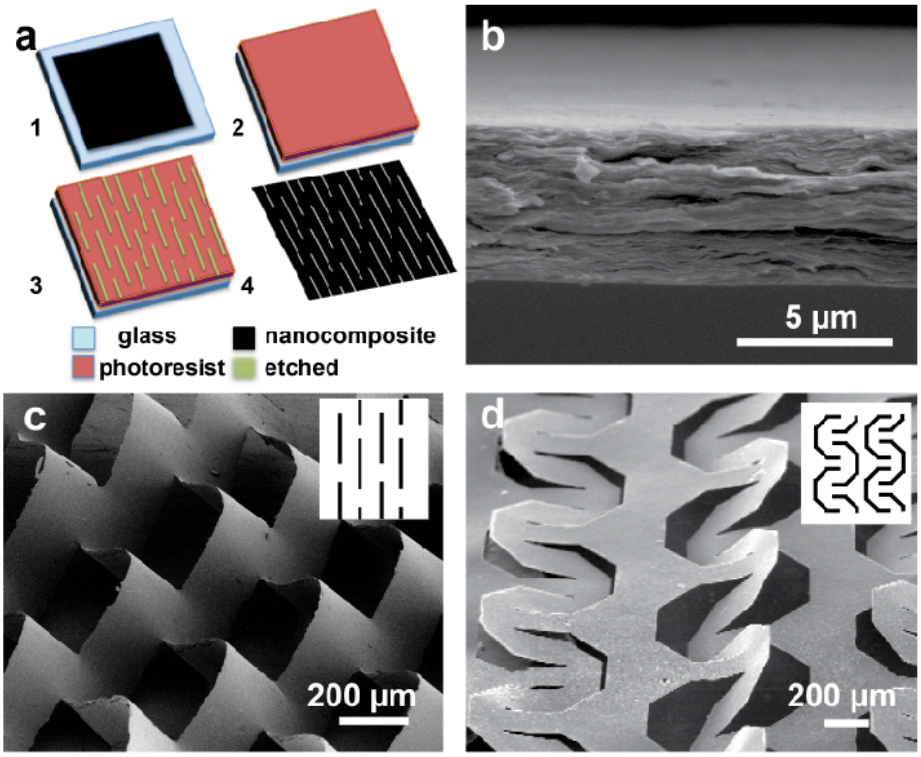

Figure 4.1: Microscale kirigami patterns. (a) Schematic of the kirigami microfabrication process. (1) A nanocomposite is deposited on a solid substrate for patterning; (2) Photoresist is deposited and developed; (3) An oxygen plasma etch through the nanocomposites creates kirigami patterns; (4) Nanocomposite sheet is detached from the substrate. (b) Scanning electron microscopy of the cross-section of a GO-PVA nanocomposites; (c, d) Two examples of microscale kirigami patterns in GO-PVA nanocomposites after photolithography. The insets show the corresponding kirigami unit cells.

4.3 Mechanical Behavior

A simple kirigami pattern consisting of straight lines in a centered rectangular arrangement (Fig. 4.2 inset) made of tracing paper (Youngs modulus, E = 1.2 GPa) provides an experimentally convenient model for this study. It has allowed us to develop a comprehensive description of deformation patterns taking place in such material. The original material without patterning shows a strain of 4% before failure; its deformation primarily involves stretching of the individual nano- micro-, and macroscale cellulose fibers (Fig.4.2 gray curve). With a single cut in the middle of the sample, the stress-strain curve shows a slight decrease of ultimate strength but otherwise behaves quite similarly to the pristine paper (dashed blue). In contrast, a sheet of the same paper with the tessellated kirigami cuts (green) shows markedly different tensile behavior, that resembles the deformation of a cellular or hierarchical material. [93, 94] The initial linear elasticity at <5% strain (Fig. 4.2 I) arises from stretching the material. As the applied tensile force exceeds a critical buckling force, the initially planar sheet starts to deform, as the thin struts formed by the cuts open up. Within this plateau of nonlinear elastic regime (Fig.4.2 II), buckling occurs at struts as they rotate to align with the applied load and deformation occurs out of the plane of the sample. During the deformation process, kirigami patterned sheets exhibit out-of-plane deflection due to mechanical bistability. This out-of-plane deflection can be used to impart additional functionality, as we demonstrate in the later part of the present study. Finally, the alignment of the struts causes the overall structure to densify perpendicular to the pulling direction (Fig. 4.2 III). Failure then begins when the ends of the cuts tear and crease due to high stress at these regions.

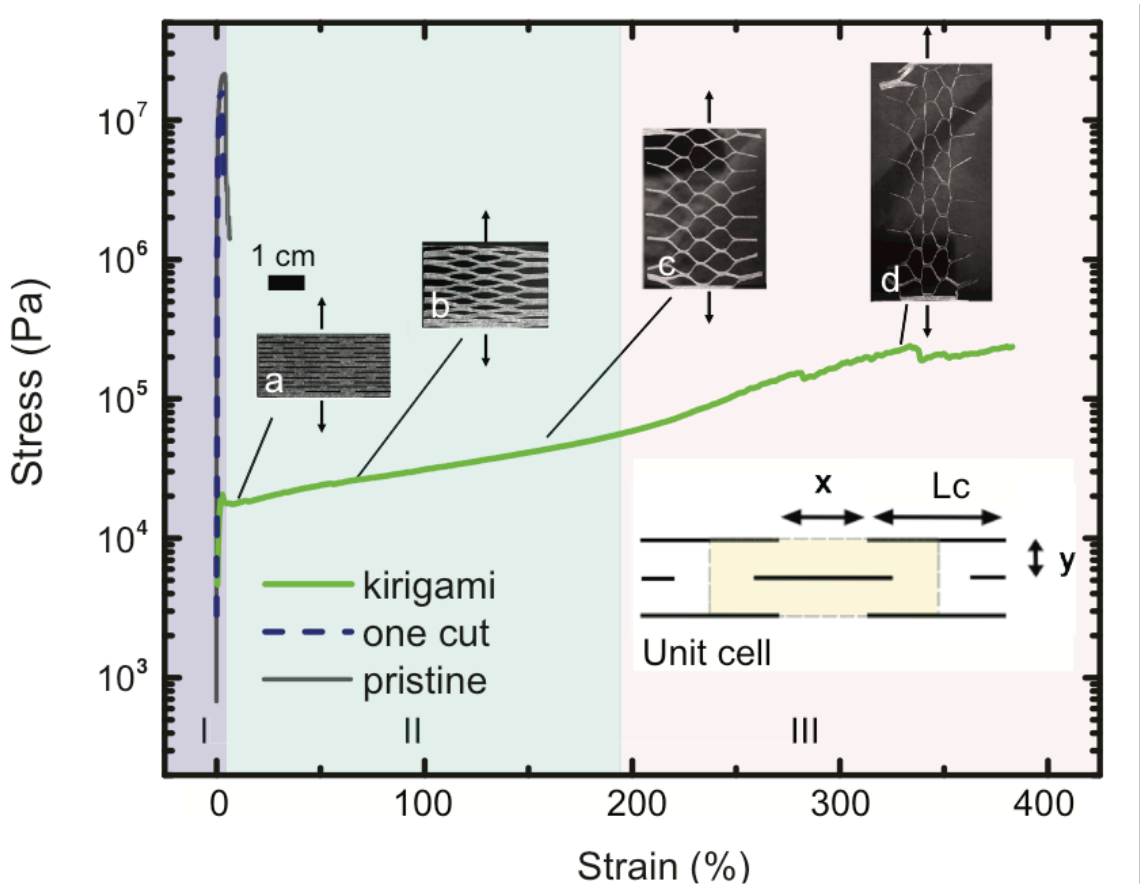

Figure 4.2: Typical stress-strain response for kirigami patterned sheets. A kirigami patterned sample (green) sustains tensile deformation to four times its original length, compared to the pristine sample (gray curve), and with just one cut in the middle (dashed blue). (I) Represents the initial elastic region; (II) Represents the nonlinear elastic region; and (III) Represents where pattern collapses. (a-d) Gradual opening of kirigami pattern. Inset: Cut pattern unit cell marked in yellow. Cuts are indicated by the black horizontal lines.

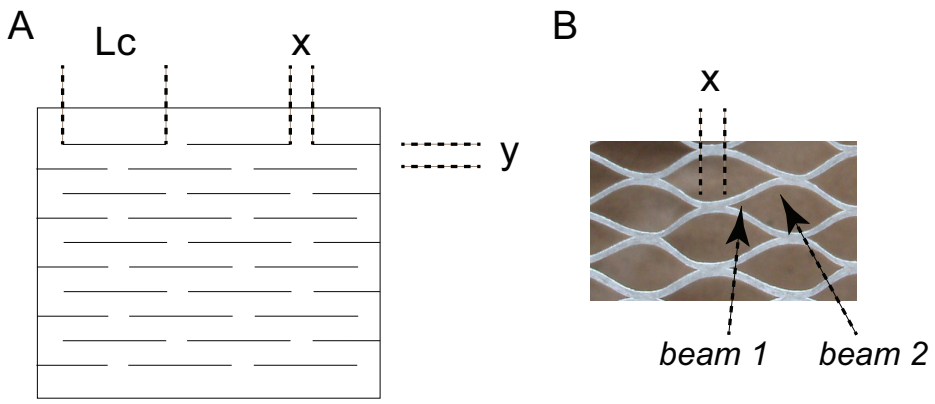

Figure 4.3: Schematics showing force analysis approximating kirigami struts as beams. (A) Kirigami geometry schematics. (B) Under a tensile force, each individual strut can be approximated as 2 beams connected in series, each with a width of $\frac{L_c-x}{4}$

4.4 Unit Cell and Buckling

We assume beam deflection in a kirigami system to analytically predict the scaling of the force associated with bistable configurations. A typical linear kirigami pattern (Figure 4.3A) has characteristic cut parameters are the cut length, L_c, and the distance between cuts in the axial, y, and transverse, x, directions. Upon stretching the sample in the axial direction, instabilities defined by the cut geometry cause shearing along the length of the cut, and a subsequent elongation of the sample and decrease in width. The circled region in Figure 4.3B is approximated as a set of two beams. This part is essentially the cut length that overlaps with the row that follows approximated as two beams connected in series (Figure 4.3C), each with a length $\frac{L_c-x}{4}$.

Using beam theory, we can relate deflection, d, and force, F, via the following equation, approximating the beams as two free-end cantilevers joined together:

$$d = \frac{FL^3}{3EI}$$

where L is the beam length, E the Youngs modulus of the material, and I the moment of inertia, where

$$I = \frac{wt^3}{12}$$

Here w is the width of the beam, and t the thickness in the direction of deflection. It follows that

$$d = \frac{4FL^3}{Ewt^3}$$

Since the two beams are connected in series, the deflection is additive such that

$$d_{total} = d_{beam1} + d_{beam2} = 2d_{beam1} = \frac{8FL^3}{Ewt^3}$$

Solving for force as a function of deflection, and substituting the kirigami unit cell parameters,

$$F_{beam} = \frac{Eyt^3}{4(\frac{L_c - x}{4})^3} = \frac{8Edyt^3}{(L_c - x)^3}$$

The total force acting on the kirigami structure is thus a sum of all the beams in the transverse direction (i.e. along the width of sample) and axial direction (i.e. along the length of sample). The beams in a given row are connected in parallel such that the forces acting on the structure for that row are additive, thus the total force, F_{total}, can be expressed in terms of force on a row F_{row}, number of row N_{row}, and the previously defined terms:

$$F_{total} = \frac{F_{row}}{N_{row}} = \frac{N_B F_{beam}}{N_{row}} = \frac{8dN_B Eyt^3}{N_{row}(L_c - x)^3}$$

The maximum extension, or attainable strain (in % strain) is the ratio between the change of length at maximum extension to the original length:

$$\%strain = \frac{\Delta L}{L_i} = \frac{L_c - x}{2y}$$

Once this maximum is reached, the final yielding will vary based on how the cuts grow.

The effect of the kirigami pattern on the overall mechanical response can be evaluated using the same beam assumption, and we find that the critical force scales with $\frac{Eyt^3}{(L_c - x)^3}$. This buckling analysis gives us an intuition on how the experimental parameters relate to the critical buckling force. It is, however, not trivial to predict the *force-displacement* relationships, or the elastic response due to the complex deformation that also involve twisting and bending. Here, FEM is useful to predict the post-buckling behavior.

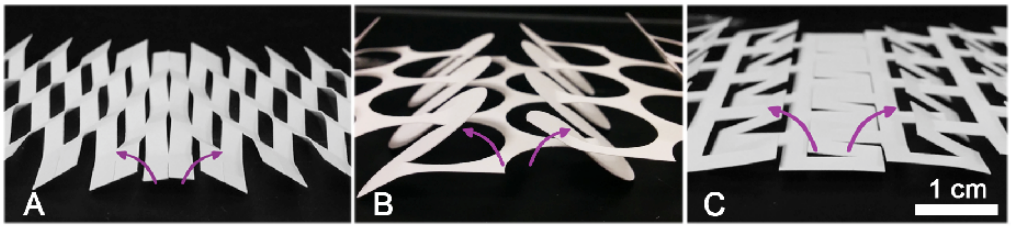

Figure 4.4: Photographs of paper samples, showing that as the sample extends under uniaxial tension, the system chooses the favorable configuration by bending out of plane. Here the sample can bend either in the clockwise or counterclockwise direction. (A) Linear pattern, (B) circular pattern, (C) square pattern.

It is important to note that this buckling behavior gives rise to a mechanical instability, where two configurations have the same energy. The out-of-plane motion can take on positive or negative rotation angle (Fig. 4.4), where the system is bistable and the final configuration is intricately related to initial and boundary conditions. Similar behavior is well-documented in other types of systems that are exploited for directed pattern transformation in dynamically tunable structures. [101, 168, 169, 170, 171, 172]

4.5 Control of Deformation

Having defined the relevant geometric and material parameters, we investigate the control over the deformation by systematically varying the kirigami unit-cell geometry in the plane view, as defined in Fig. 4.6 (lower insets), for horizontal spacing x, vertical spacing y, and cut length L_c, respectively. As expected, the critical buckling load and the size of the nonlinear elastic region - which dictates the maximum extension of the samples at failure - are strongly affected by the unit-cell geometry (Fig.4.6 a-c). The critical buckling load marks the onset of buckling, where the initial

elastic linear regime transitions to the nonlinear regime. Our experimental results show that an increase in x-spacing shifts the stressstrain curve up, corresponding to higher critical buckling loads. An increase in y-spacing decreases the maximum extension and increases the critical buckling load, as expected from the beam analysis. An increased L_c softens the material, resulting in a lower critical buckling load and higher extensibility. Generally, an increased spacing between the cuts makes the sheet more rigid and imparts a higher critical buckling load, whereas increasing the cut length weakens the material, lowers its critical buckling load, and increases its extensibility. In contrast to the usual trade-off between strength and extensibility, an increased x-spacing does not exhibit this trade-off. This is because each cut is able to grow, or tear, along the cut length until neighboring (in the strain-transverse direction) cuts begin to coalesce, without the overall structure failing. In the process of tearing and final coalescence along the cuts, fracture energy is dissipated while allowing the sheet to extend even further. Hence, the increase of toughness here is related to the distance between the structural features, demonstrating a toughening strategy on a higher length scale. This suggests that the relationship between pattern spacing and mechanical response may be extended to other length scales and materials where high strains are desirable. The uniformity of the material is the only structural limitation for such scaling behavior that we foresee at present. The cuts need only to be larger than the typical variations in materials composition and properties of the sheet.

The key trends observed in our experiments are replicated by FEM analysis (Fig. 4.6ac insets), revealing geometric parameters that are in agreement with our intuitive understanding and the beam deflection analysis. We note that FEM accurately reproduces the general stressstrain response and the experimentally observed effects of geometrical parameters. Conversely, FEM predictions underestimate the buckling load. These deviations are associated with microscale deformations of the

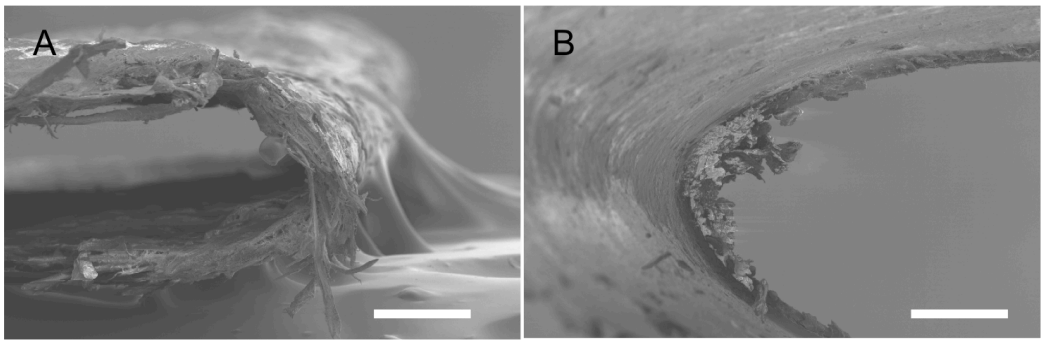

Figure 4.5: SEM images showing the morphology of (A) the paper sample and (B) the polyimide sample.

material. For example, the finite-element model does not describe the fibrous morphology observed in typical paper samples (Fig. 4.5A). However, it is possible to use a uniform polyimide sample that does not have the fibrous morphology, which reflect quantitative agreement with between FEM and experimental data (Fig. 4.5B). Confirming the source of the deviations, we achieved quantitative agreement with our experiments by using a uniform crystalline polyimide film, laser-cut to render clean, even widths. These samples were also tested for fatigue life up to 1,000 cycles running to 70% strain, with an 18% strain energy fade. [173, 174] This result shows remarkable damage tolerance and suggests potential reversible and reconfigurable applications for the kirigami patterns.

The FEM results show that the applied load is distributed uniformly throughout the kirigami sheets, rather than concentrating on singularities with random initiation sites (Fig.4.7).Thus, highs train is accommodated to improve damage tolerance despite multiple defect sites. This deformation scheme contrasts with the deformation of typical stiff materials, where the presence of any defect acts as a stress concentrator from which cracks propagate and lead to fracture. Considering the deformation in terms of stress fields, we find that kirigami patterns can be used to dictate stress concentrations and effectively control deformation. To further reduce the loads at the

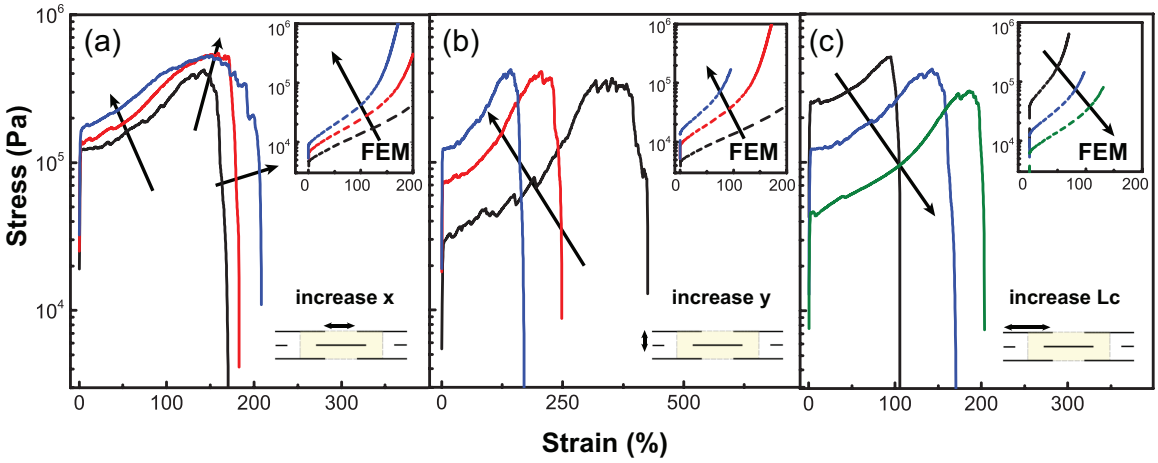

Figure 4.6: Experimental and FEM-calculated stress-strain curves for macroscale kirigami sheets with variable unit-cell parameters. (a) Horizontal separation x bewteen the cuts. (b) Vertical separation y between the cuts. (c) Cut length L_c. Figures show the experimental results and insets show results from FEM.

cuts, we employ a technique widely used in fracture mechanics - blunting the crack tip using a stress distributing geometry, such as circles (Fig.4.8). These circular features effectively delay the onset of tearing and lead to a larger operating window for the nonlinear elastic region.

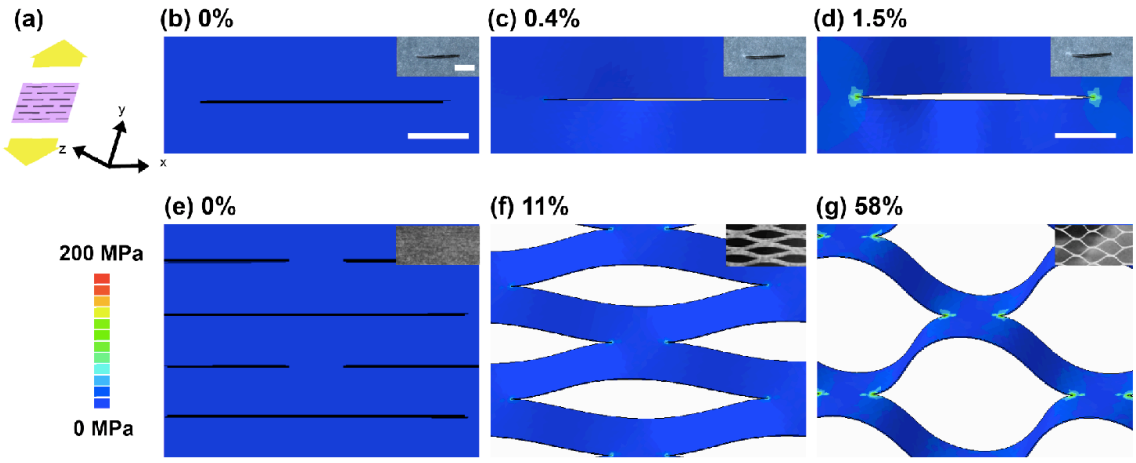

Figure 4.7: Stress concentration visualization in FEM. (a) Schematic of loading direction with respect to the unit cell. (b-d) FEM snapshots showing stress distribution of sheet containing a single cut a t the strain level indicated. (e-g) Stress distribution of periodic kirigami cut at the strain levels indicated. Insets in b-g show the corresponding samples. Scale bar, 2mm.

4.6 Strain-Conductivity Relationship

Traditionally, stretchable conductive nanocomposites suffer unpredictable strain effects due to changes in the conductive pathway during deformation, leading to conductivities that fall as much as 2 orders of magnitude depending on the amount of loading and the number of stretching cycles. The strain effects thus depend on the microstructure of the material and the strain history. The alternative scheme to make stretchable conducting nanocomposites using the kirigami method can simultaneously enable large extensions on a variety of materials and eliminate the unpredictable effects under large strains over many cycles. The large strains enabled by the kirigami structures described in this study can make the deformation to the point of failure deterministic. Kirigami nanocomposites may have strain-invariant electrical conductance, potentially useful in a variety of devices, including stretchable current collectors and electrodes.

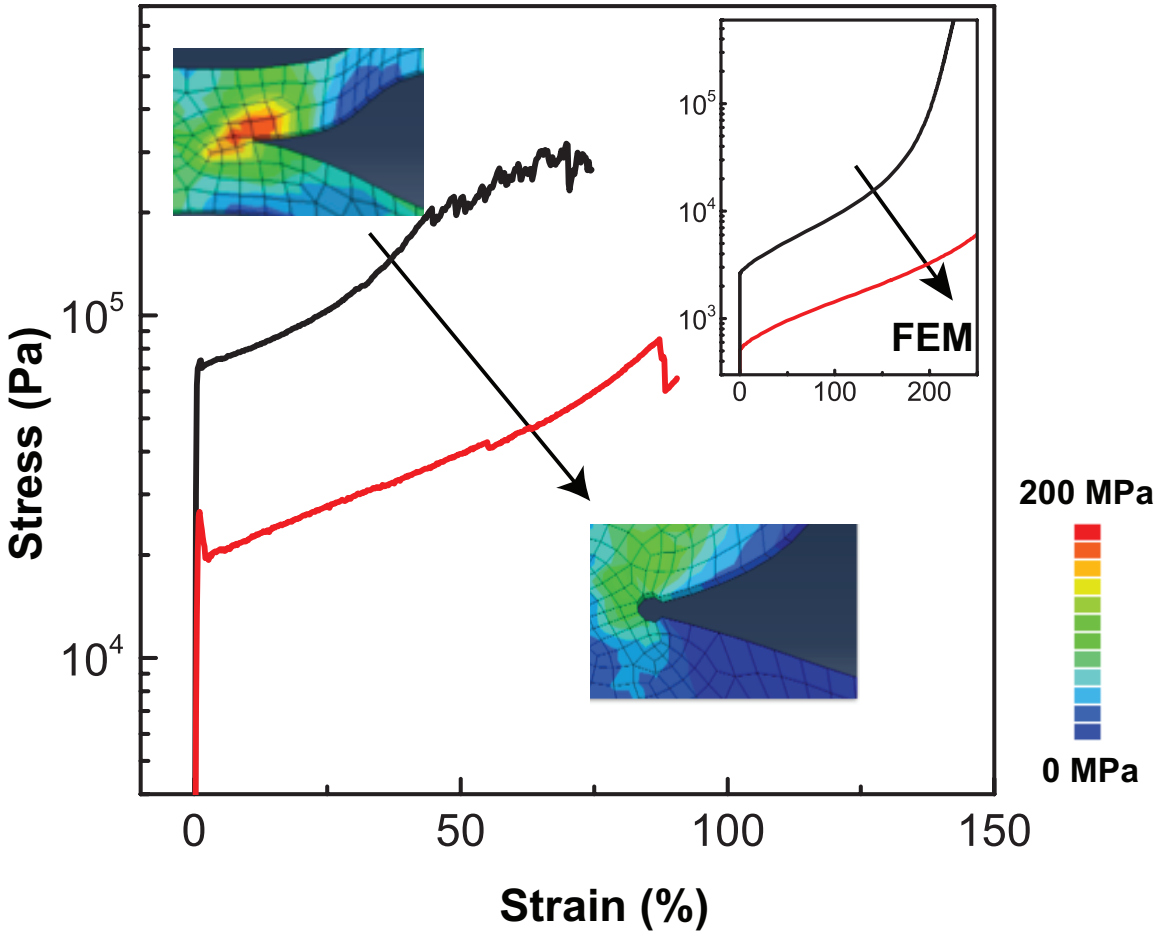

Figure 4.8: Blunting the cut edge in the form of a circle at the edge of the cuts can further distribute the stress at each cut edge. The plot shows the sample with (red) and without (black) the stress distributing geometry. The effective stress at the crack tip decreases, as seen in the FEM insets.

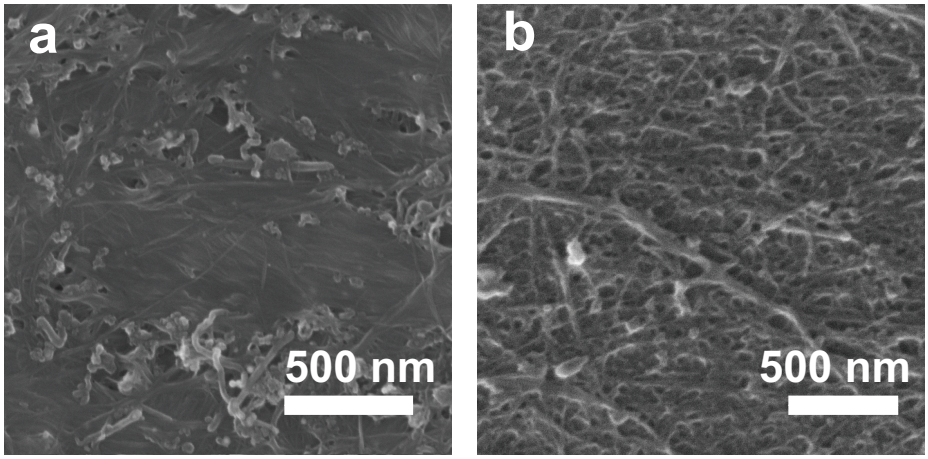

Figure 4.9: SEM images showing the microstructure of CNT nanocomposite on (a) paper, fabricated by vacuum infiltration, and (b) on parylene, fabricated by LBL.

The large strains enabled by the kirigami structures described in this study may have strain-invariant electrical conductance, potentially useful in a variety of devices, including stretchable current collectors and electrodes. To do so, we infiltrate tracing paper with well-dispersed single-walled carbon nanotubes. Kirigami patterning is similarly introduced on the CNT infiltrated paper. For comparison, an LBL-assembled $(CNT/PVA)_{30}$ was fabricated on a 5-m parylene. (Fig. 4.9)With the kirigami patterns, the yield strain increases from around 5% to 290% and 200% for the paper and LBL nanocomposite, respectively. The conductance does not change significantly during stretching for both the paper and LBL nanocomposites (Fig. 4.11b), indicating that the presence of the patterned notches accommodates strain while maintaining a conductive network provided by the CNT. In both cases the strain obtained is 20-30 times greater than for similar composites without the notch patterns. [175]

The unique combination of high strain and high conductivity observed for 3D kirigami nanocomposites allows us to use them as electrodes for tunable plasma discharge inside an argon-filled glass tube. We use a custom glass plasma chamber (Fig.

4.10). The top is fitted with a hollow glass tube to allow for in situ strain tuning capabilities while the voltage is applied onto the kirigami electrode. The ground is attached on one side of the glass chamber for observation of changes in plasma discharge under different strain levels. At constant voltage and pressure, the electric field concentrates at the sharp apices that arise from the strain-induced out-of-plane deformation (Fig. 4.11c). At constant voltage and pressure, the electric field concentrates at the sharp apices that arise from the strain-induced out-of-plane deformation. Effectively, the increased strain increases the roughness of the electrode, which lowers the corona onset voltage. [176] Hence, as the strain level is increased, we visually observe a higher degree of local ionization and plasma intensity resulting from increased recombination of ionized species. The development of tunable electrodes opens up the possibility of many useful new applications in plasma materials treatment, processing, deposition, plasma induced airflow, and more.

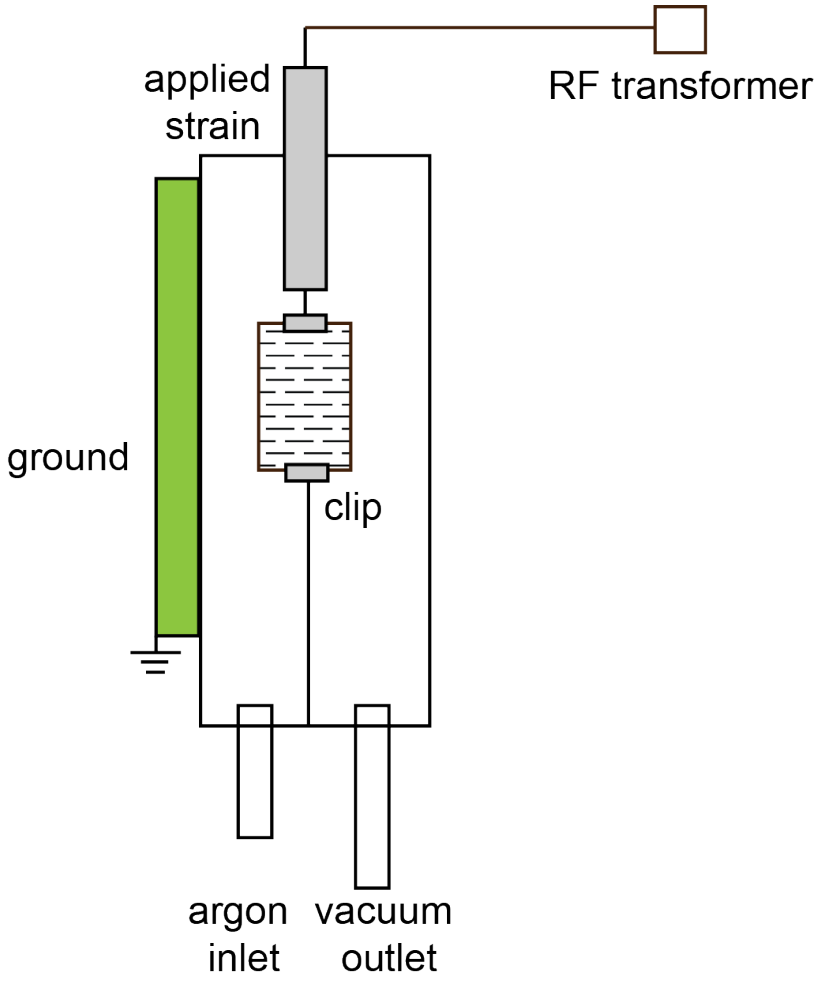

Figure 4.10: Schematics of the custom-made plasma chamber, with in-situ tunable strain, argon inlet, vacuum outlet, and an RF transformer to apply the voltage.

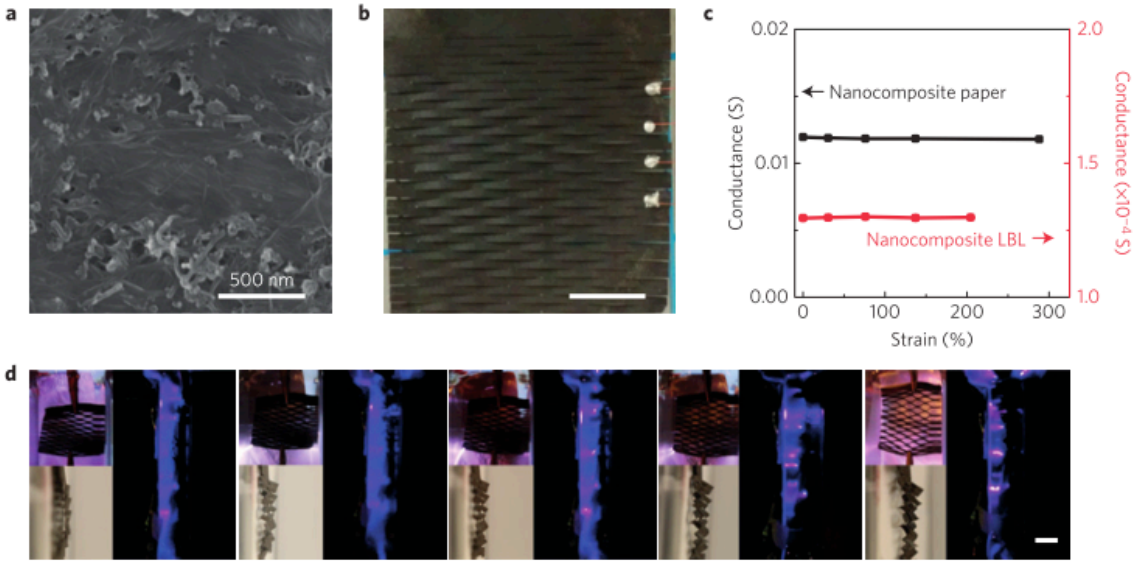

Figure 4.11: Strain-invariant conductance on CNT nanocomposites as an electrode. (a) Scanning electron micrograph of CNT nanocomposite sheet made by vacuum infiltration. (b) Kirigami pattern introduced on a CNT infiltrated paper. (c) Conductance versus strain data for kirigami on paper (infiltrated CNT) and LBL on parylene, and (d) Plasma patterns generated on a krigami electrode at strain levels of 5, 10, 15, 20, and 25% (left to right); upper and lower insets show front and side views, respectively. (b, d) Scale bars, 1 cm.

And finally, we tested the kirigami samples by cyclically loading nanocomposite paper to 200% strain over 4 cycles, and a polyimide sample to 60% strain over 1000 cycles (Fig. 4.12). In the nanocomposite paper, we see elastic energy recovery of 75% on the first run, and around 90% on the subsequent runs. It appears that the in the first run, some elastic energy is not recoverable due to permanent deformation occurring on the microstructural level. The polyimide sample experiences a fall in recoverable energy (the area under the stress-strain curve) in the first 100 cycles. As the number of cycle increases, the recoverable strain energy appears to flatten out. For use in a practical device, some of the critical design parameters for a cyclically loaded kirigami device will include the total deforming area, which will have to do with the fraction of the overall area undergoing deformation, and the thickness of the

film, which will determine the recoverable bending radius. More mechanical fatigue data will further elucidate how the kirigami patterning influences fatigue life. Other designs of kirigami that allow multi-directional loading and the cut edge blunting strategy mentioned previously can also be an effective ways to widen the applicability of kirigami patterning.

4.7 Conclusion

In this chapter we have presented a framework to directly design deformation within a nanocomposite and delocalize stress distribution using the kirigami patterning technique and thus eliminating the unpredictable strain effects in nanocomposites. We also demonstrate the combination of the control of component in nanocomposite and its architecture via kirigami. This strategy allows us to have strain-invariant conductance within the material over a range of strain up to several times the ultimate strain of the material, depending on the cut geometry.

In contrast to molecular or nanoscale manipulation of strain, we show that it is possible to control deformation in materials with top-down kirigami patterning, which can be extended tom ultiple length scales. The new insights obtained here may bridge the gap between nanoscale and macroscale strain engineering, as well as enable novel engineering applications in which out-of-plane deflection can be controlled to create multiscale, reconfigurable structures. Kirigami nanocomposites may find potential use in radio-frequency plasma applications, including surface treatment, materials processing, displays, radar phase arrays, ozone production and corona-induced airflow. Deformable electrodes that can withstand a wide range of strains can also be extended to a variety of flexible-electronic technologies beyond plasma processes.

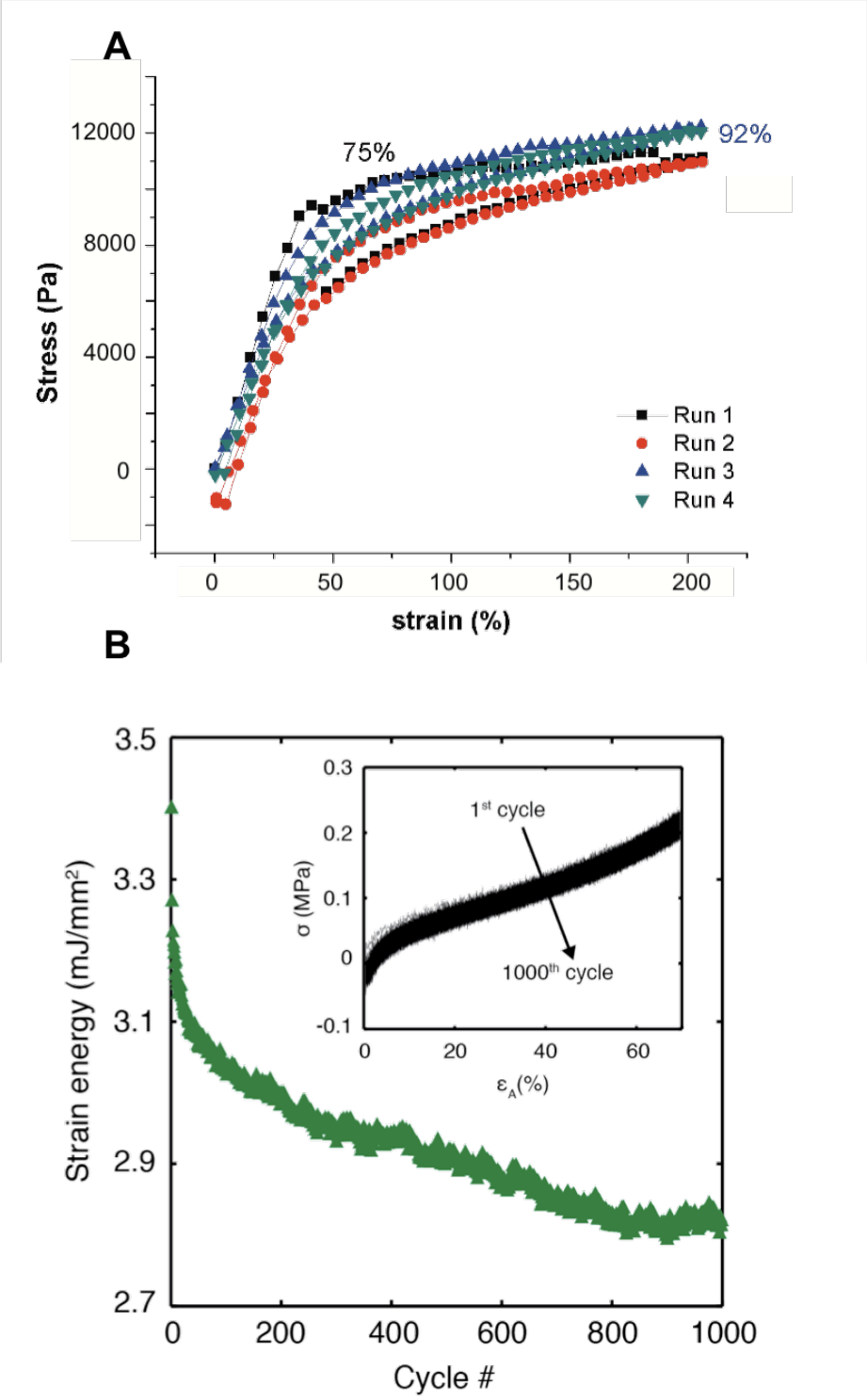

Figure 4.12: Cyclic loading data for the nanocomposite paper and polyimide, showing elastic energy recovery. (A) Nanocomposite paper tested over 4 cycles, and (B) polyimide sample tested over 1000 cycles, plotting the recovered strain energy versus cycle number. Inset, the stress-strain data from the first to 1000^{th} cycle.

CHAPTER V

Tunable Kirigami

In the previous chapter we have described kirigami patterned structures and proposed using kirigami as a way to engineer elasticity and deformation. In this chapter we focus on how to use these kirigami patterned structures for dynamic applications. Recent development in kirigami has fueled research interest in using these mechanical structures for dynamic purposes, including solar tracking [174] and optical transmission window. [177]

We propose applying the kirigami approach to explore the dynamic tuning of radio frequency (RF) plasma because of two primary reasons. The first is that the phenomenon is visible, making the observation convenient - within a plasma, inelastic collisions occur to emit radiation of light. The second is that dynamic applications can have profound technological significance when applied to plasma processes, and demonstration of dynamic tuning will have significant impact in a myriad of materials processing methods currently employed in industry. With the recent development on plasma actuators to control airflow around aerodynamic surfaces, it is anticipated that kirigami electrodes may find critical applications there. We conclude with a few remarks on some foreseeable future directions in tunable kirigami.

5.1 Background

A plasma is a quasi-neutral ionized gas system containing equal number densities of electrically charged constituents, which are electrons and ions. The term *plasma* was first introduced by Langmuir [178] in 1927 to describe the gaseous fluid carrying electrons and ions, for its similarity to how plasma in blood carries the various blood cells. During excitation, a plasma is sustained by electron-neutral dissociative ionization. Within a plasma, the electrons move much faster compared to the ions and collide with one another as they move around in space. During this process, either elastic or inelastic collision can occur. Elastic collisions lead to energy transfer and dissipation but the total kinetic energy remains the same:

$$Ar^0 + e^- \rightarrow Ar^0 + e^-.$$

In contrast, inelastic scattering is responsible for excitation

$$e + Ar \rightarrow Ar^* + e$$

or electronic transitions

$$Ar^+ + e^- \rightarrow Ar^* + e \rightarrow Ar + e + h\nu$$

corresponding to

$$3p^6 \rightarrow 3p^5 4s^1.$$

Here, positive argon ion can interact with an electron and undergo an electronic transition in the outer shell, which emits a photon with the characteristic purple light.

Plasma processes have found important roles in industrial applications, particularly in electronics and materials processing, [179] as briefly alluded to in Chapter II. Depending on the interactions between the reactive ions and the material, a few plasma-material processes can occur, including ablation, etching, deposition, or chemical and physical modification due to particles and radiation from the plasma. These effects have sustained the production high powered integrated circuits, further underscoring the importance of these controlled processes.

Hence, by investigating the effects of strain tuning of a kirigami electrode in a plasma system, we can visualize the effects easily and there is a number of industrial applications associated with tunable plasma electrodes. Further, the plasma parameters can be quantified using a Langmuir probe, which measures the current at various voltages. From the current-voltage ($I - V$) characteristics, the electron and ion currents, densities, and electron temperature can be extracted.

5.2 Experimental Method

As a first demonstration, we use a 25 μm Kapton polyimide film with e-beam evaporated 5 nm Cr and 50 nm Au for electrical conductivity and contact between the film and the chuck in a radio frequency (RF) plasma generator. The kirigami pattern is introduced using a laser cutting tool (WKLaser LC1280) at 40 W, the cut spacings at 2 mm and L_c at 1 cm.

At a frequency of 13.56 MHz, using argon gas at 500 mTorr and 50 W, we are able to sustain a plasma. The strain level on the kirigami sample is varied from 0% strain to 20% strain. The $I - V$ curves are obtained at each strain level, averaged

over 5 times. The bulk plasma parameters are automatically extracted.

5.3 Strain-Tunable Plasma Parameters

The extracted plasma parameters show increase of number and current density for both the ions and the electrons within the plasma with increasing strain. At higher strain levels, the localization of electric field on the sharp edges in the kirigami sample tends to cause severe arcing, which can damage the sample. At higher strains, the plasma tends to be also unstable. However, it can be seen qualitatively (Fig. 5.1) and quantitatively (Fig. 5.2) that the tuning of electric field due to the change in topology can induce changes in bulk plasma properties.

Typically to tune these properties, one can change the RF power and gas pressure. It is conceivable that fine tuning the geometry, length scale, and operating power, one can use mechanical strain as a knob to tune bulk plasma properties. Additionally, the local electric field is inversely related to the radius of curvature. The radius of curvature decreases as the strain is increased. Therefore, the strain-tuning of kirigami can effectively alter the local electric field due to the out-of-plane deformation, and in turn modulate the power density of the plasma, and concentrate the electric field at the sharp electrode edges.

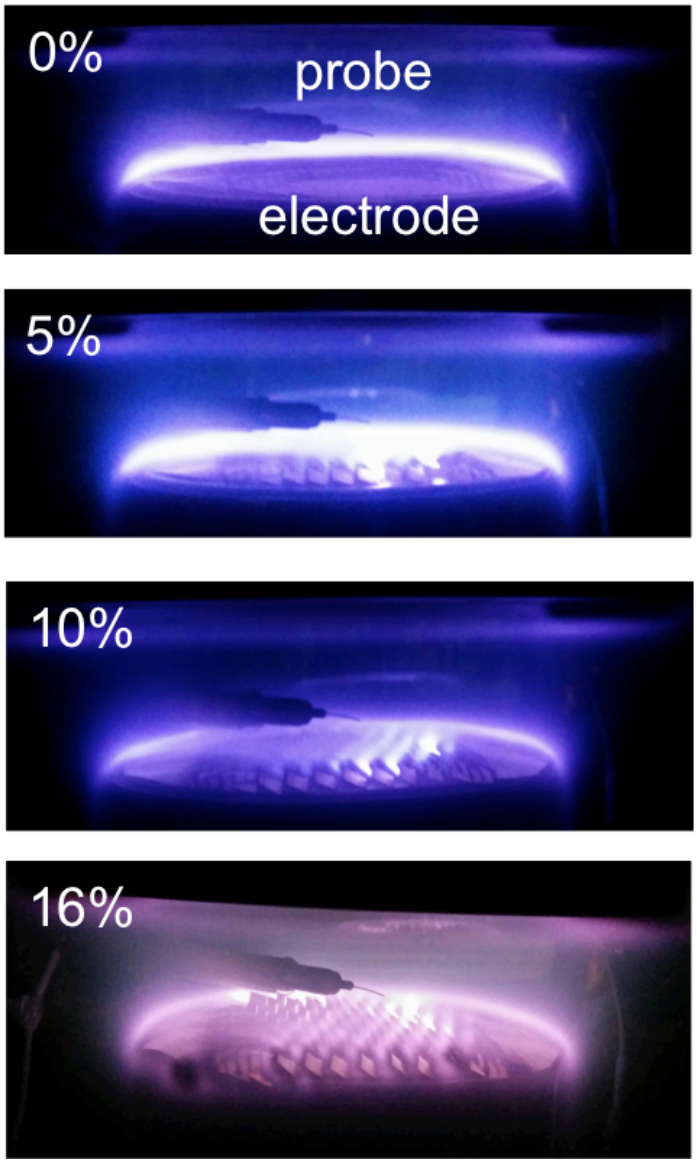

Figure 5.1: Qualitative data showing stress-tunable plasma properties at strain levels of 0, 5, 10, and 16%.

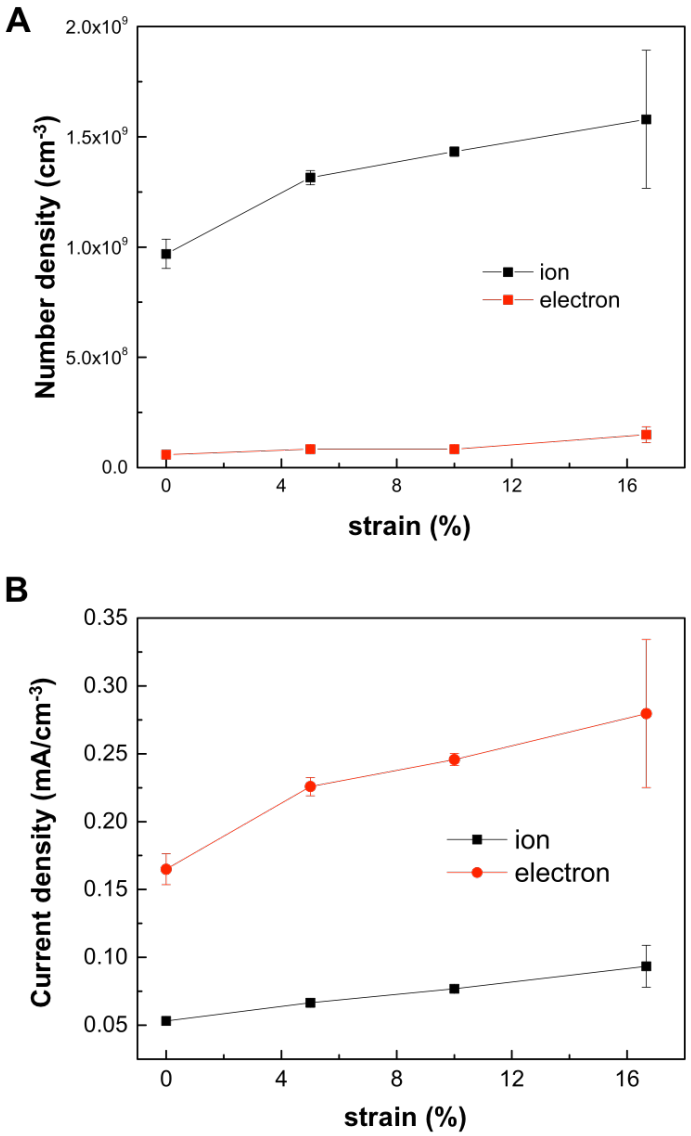

Figure 5.2: Quantitative data showing stress-tunable plasma properties. (A) Number density versus applied strain, (B) Current density versus applied strain. Black: for ion species, red: electrons.

5.4 Conclusion

We have shown that it is possible to tune bulk plasma properties by altering the local electric field. Besides the number density and current density of the charged species, the spatial and temporal structure of the plasma will can be further explored for the emerging application in, for example, aerodynamic plasma actuator. Recent interest in dielectric barrier discharge plasma has been focused on aerodynamic applications. The plasma discharge strongly influences the surrounding airflow, and can be used to control aerodynamic surfaces without the use of mechanical parts. [180, 181, 182]

Beyond plasma parameters, it is also possible to use the kirigami technique to design chiral materials. The subject is outside the scope of this thesis, however, it is worth briefly noting the literature on kagome [183] and auxetic lattices. [184, 171] Certain cellular lattices and the kagome lattice - a tiling pattern in woven basketry and certain crystal structures - are capable of chiral transitions from rotation. An example of the chiral kirigami design is illustrated (Fig. 5.3). More on the design and mechanics of these rotating structures will need to be investigated for application of kirigami chiral materials.

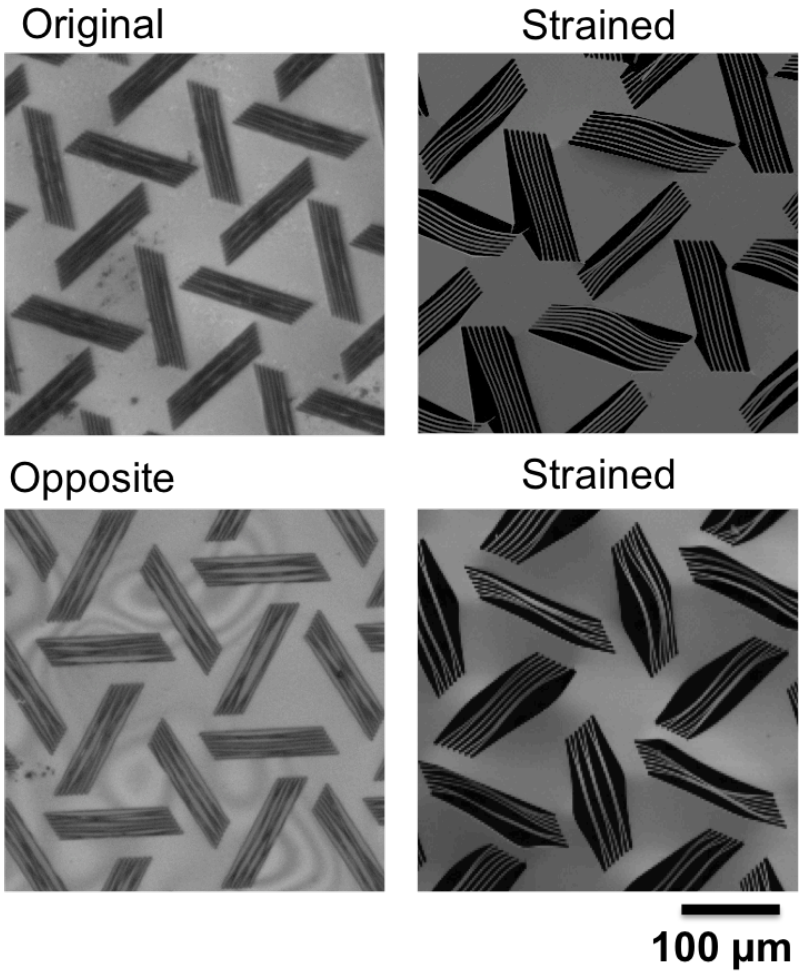

Figure 5.3: Rotating kirigami structures with out-of-plane twists.

CHAPTER VI

Summary and Future Directions

The field of engineering origami and kirigami has a relatively short history, and is a rapidly developing area. Balanced by geometry, the potential for reconfigurability sits in the intersection between materials and mechanics. Since the early studies on deployable structures for aerospace applications by Miura [3, 4] and others, [16] research in engineering foldable and morphing structures have translated into diverging and fruitful areas, including 3D microfabrication, bio-mimicry, and metamaterials.

In this work, we have focused on composite systems and described coupling materials and mechanics to engineer functionalities. In Chapter III, we described an approach to create a layer-by-layer assembled humidity-responsive mechanical actuator. Electrostatically held water can reversibly go in and out of the system. A bilayer scheme is employed, where the differential response between the two layers with changes in ambient humidity effectively helps us create gentle mechanical motion on the order of seconds in response time. Additionally, inkjet patterning allows us to place the active material precisely in space. In Chapters IV and V, we described an approach to control strain-property relationship by controlling the deformation via kirigami patterning. In materials engineering, one typically tunes properties of mate-

rials by atomic and microstructural manipulation; here we show that the deformation of the material is controlled by the geometry to enable functionality.

Besides the mechanistic design rules and the materials involved, smart materials of the future using these strategies would also require considerations of scale, both in time and in space. The response time, τ, for example, will influence how materials are being used, beyond the start and end states. The response time may also be a function of the length scale in question. Future studies can be guided by thinking about the time scale and length scale of responsiveness. These will determine what kinds of applications are possible. In the following sections, we discuss future work in the context of time scale and length scale. Finally, we will conclude with a discussion on the design of deformation.

6.1 Time Scale

In nature, the origami folding scheme based on hydration is also seen in pinecones, wheat awn, and many seed dispersal systems. [185, 186, 187] Bilayers of materials with different swelling properties controls the hydroscopic actuators, much like in a thin bimetallic metal strip. [48] These systems are entirely driven by the ambient humidity and do not require electrical control, making them suitable for passive design elements driven by environmental changes.

The gentle movement due to multilayer hydration is in contrast to the fast movement observed in the Venus fly trap. The response time on the order of 10^2 milliseconds is possible because of a buckling bistability, where the structure has two mechanically stable configurations. Holmes and Crosby [169] investigated the

response time by mimicking the Venus fly trap with PDMS, an elastomeric material. Much like many systems described in this work and in the referenced literature, the mechanical instability is a balance between materials properties and geometry. Similar to bilayer bending, buckling is also dependent on the material thickness (t) and Youngs modulus (E), and thus the system can be scaled up to larger systems (meter scale) and down (micro- to nanometer scale). Here, τ is given by:

$$\tau \approx \frac{\mu t^2}{kE}$$

where μ is the viscosity of the swelling fluid in the system, and k is the hydraulic permeability, for a buckling shell encapsulating a fluid-filled cell. This example demonstrate using mechanical instability to control the response time in a responsive system.

Important to note, however, for bilayer bending schemes described in these studies, the processes are controlled by diffusion (of ions, [31] water, [140] or heat [132]). In this case, microscale actuators works well, but for larger scale systems, the transport pathway will have to be engineered. Hence the length scale must be given consideration for successful design.

6.2 Length Scale

In contrast to the length scale dependency in transport phenomena, in geometric systems the length scale independence of the governing physical laws can

make them suitable for the development of mechanical metamaterials. In creating stimuli responsive materials, the consideration of length scale is also related to how the structure is actuated and the resulting application. In the integrated circuits world, reducing in length scale relate to profit. In contrast, in the world of responsive systems, length scale tells us which functional properties can be controlled. For example, in the macroscale, kirigami has recently been demonstrated for solar tracking application. [174] In the sub-millimeter scale, the kirigami technique combined with strained polymer has been used to organize microarrays. [177] These are relatively new studies. In Chapter IV, we have discussed controlling microscale deformation to maintain conductance throughout the entire range of strain. This is one example of how the control of deformation at a specific length scale can help control functional properties. Ongoing work in this area can extended to sub-micron scales and smaller, with application in the control of optical properties, including chiral materials and diffraction gratings.

Mechanical instability is intricately related to geometry. Over the years, the Bertoldi group has studied a range of architectured shell structures with negative Poisson's ratio in the form of sheets and buckling three-dimensional structures termed "Buckliballs". [101, 188, 189] Similar to the Miura-ori, the mechanical properties arise primarily from the geometry. Experimental demonstrations are typically silicone-based elastomers and hydrogels because of the ease of fabrication - usually by a molding process - and reversibility. Future work in incorporating nanomaterials can potentially couple the well-described mechanics with other functional properties in various length scales and time scales, and is expected to have important implications in smart material systems. [190]

6.3 Design of Deformation

Further, designing deformation via kirigami as we have discussed in Chapter IV has potential applications in engineering mechanical properties and extending the fatigue life of stretchable devices. For example, we have described in Chapter I that microfabricated biomedical devices have seen tremendous growth in recent years. One critical materials challenge in this area is on matching the mechanical property of device with that of tissues, while maintaining functionality. This is especially important for implants in the brain - a neural probe may be inserted within the brain, but mismatched mechanical properties between the probe and the tissue would cause chronic inflammation despite otherwise minimal biological response. Typically, tissues have Young's modulus (E) on the order of kPa, while microfabricated silicon electrodes are on the order of GPa. Currently, to overcome this problem, several studies have looked into creating thin structures supported on flexible substrates. [50] These structures are typically buckled, [163] serpentine, [191, 192] or hierarchical, [165] and it is also possible to directly evaporate thin metal films onto flexible substrates. By using the kirigami approach, one can anticipate engineering the desired mechanical response directly into the material. Because of the structural deformation, it is possible to accommodate strains and minimize strain effects typically observed in stretchable conducting nanocomposites. Using computational modeling, it is expected that a range of geometries and desired mechanical response can be quickly explored.

Focusing on the design of deformation, the kirigami approach described in this work can be thought of as a two dimensional case to design deformation pathway, enabled by buckling out of plane. Extrapolating this design strategy to a three-dimensional case, architectured materials such as microlattices [193, 194, 195, 196, 197] also demonstrate a pathway to design the mode of deformation under a compres-

sive mechanical load. Typically, metallic and ceramic microlattices are fabricated by uniformly coating a template constructed using two-photon lithography direct laser writing. The template is later removed, leaving the hollow microlattices. Because of the structural hierarchy from the centimeter to nanometer scale, metal microlattices are capable of complete recovery of compressive load. More recently, ceramic microlattices have also been made by atomic layer deposition (ALD) or sintering of nanoparticle-loaded resins. [194] Whereas ceramic materials typically suffer catastrophic brittle failure, the microlattice architecture effectively control the deformation mode, resulting in materials that can withstand recoverable 50% compressive load. Studies on cellular solids highlight using the lattice structures such as octet-truss to control the deformation mechanism, which result in their high strength. The lightweight, high strength, and elastic recovery afforded by the AM microlattices are desirable for material designs that go through cyclic loads.

In both the 2D kirigami and the 3D microlattice examples, the periodic structures give rise to the control of the deformation, such that stresses concentrate at designated spatial positions, as opposed to stochastically distributed defects and voids. Periodic and architectured structures offer an approach to engineer the deformation mechanism, such that two goals can be realized. The first is that these structures have desirable strength-to-weight ratio. The second is that the hierarchical structuring can enable control of deformation mechanism and recovery in the brittle materials. Anticipated relevant parameters include thickness-to-width ratio of the deforming members, scales of hierarchy, and geometry. Also expected is that the control of deformation established by computation and confirmed by experiment can provide rational design of novel architectured materials that operate within the range of the engineered deformation.

Finally, in conjunction with the design of deformation, kirigami and origami engineering have been of research interest because the possibility to create out-of-plane deformation, or the "pop-up" effect. Driven by the minimization of strain energy, buckling deformation seen in kirigami, wrinkling observed in hard skin on flexible substrate, and self-positioning of bilayers are all examples of deformation in the third dimension. Engineering of the pop-up effect on multiple length scales is expected to have applications in aerodynamic skin, pattern transformation, and surface engineering. Continued growth in engineering origami and kirigami can be anticipated. The time and length scale will need to be taken in consideration along with the mechanics of deformation. Designing deformation will yield an effective engineering approach toward next generation of tunable and multifunctional materials.

BIBLIOGRAPHY

BIBLIOGRAPHY

[1] Thomas Francis Carter. *The invention of printing in China and its spread westward*. The Ronald Press Company, New York, 2nd edition, 1955.

[2] Unknown. *Hiden senbazuru orikata*. Japan, 1797.

[3] K Miura. Proposition of Pseudo-Cylindrical Concave Polyhedral Shells. *Institute of Space and Aeronautical Science Report*, pages 141–163, 1969.

[4] K Miura. PCCP Shell. In H.R. Drew and S. Pellegrino, editors, *New Approaches to Structural Mechanics, Shells, and Biological Structures*. Springer Science, 2002.

[5] Yutaka Nishiyama. Miura folding: applying origami to space exploration. *International Journal of Pure and Applied Mathematics*, 79(2):269–279, 2012.

[6] Ramses V. Martinez, Carina R. Fish, Xin Chen, and George M. Whitesides. Elastomeric Origami: Programmable Paper-Elastomer Composites as Pneumatic Actuators. *Advanced Functional Materials*, 22(7):1376–1384, apr 2012.

[7] D. H. Gracias, J Tien, T. L. Breen, C Hsu, and George M. Whitesides. Forming Electrical Networks in Three Dimensions by Self-Assembly. *Science*, 289:1170–1172, 2000.

[8] Jose M. Zanardi Ocampo, Pablo O Vaccaro, Thomas Fleischmann, Te-sheng Wang, Kazuyoshi Kubota, Tahito Aida, Toshiaki Ohnishi, Akira Sugimura, Ryo Izumoto, Makoto Hosoda, and Shigeki Nashima. Optical actuation of micromirrors fabricated by the micro-origami technique. *Applied Physics Letters*, 83(18):3647, 2003.

[9] Timothy G Leong, Paul A Lester, Travis L Koh, Emma K Call, and David H Gracias. Surface tension-driven self-folding polyhedra. *Langmuir*, 23(17):8747–8751, 2007.

[10] Z. Y. Wei, Z. V. Guo, L. Dudte, H. Y. Liang, and L. Mahadevan. Geometric Mechanics of Periodic Pleated Origami. *Physical Review Letters*, 110(21):215501, may 2013.

[11] Toen Castle, Yigil Cho, Xingting Gong, Euiyeon Jung, Daniel M. Sussman, Shu Yang, and Randall D. Kamien. Making the Cut: Lattice Kirigami Rules. *Physical Review Letters*, 113(24):245502, dec 2014.

[12] Kazuya Saito, Akira Tsukahara, and Yoji Okabe. New Deployable Structures Based on an Elastic Origami Model. *Journal of Mechanical Design*, 137(2):021402, feb 2015.

[13] By Thomas W Ebbesen and Hidefumi Hiura. Graphene in 3-Dimensions : Towards Graphite Origami. *Advanced Materials*, 7(6):582–586, 1995.

[14] Steven Cranford, Dipanjan Sen, and Markus J Buehler. Meso-origami: Folding multilayer graphene sheets. *Applied Physics Letters*, 95(12):123121, 2009.

[15] Melina Blees, Peter Rose, Arthur Barnard, Samantha Roberts, and Paul L. McEuen. Graphene Kirigami, 2014.

[16] Tomohiro Tachi. Generalization of Rigid Foldable Quadrilateral Mesh Origami. *Proceedings of the International Association for Shell and Spatial Structures (IASS) Symposium*, (October):2287–2294, 2009.

[17] Erik D Demaine. Folding and Unfolding Linkages, Paper, and Polyhedra. *Revised Papers from the Japan Conference on Discrete and Computational Geometry2*, 2098:113–124, 2000.

[18] Mark Schenk and Simon D Guest. Geometry of Miura-folded metamaterials. *Proceedings of the National Academy of Sciences of the United States of America*, 110(9):3276–81, feb 2013.

[19] Robert J. Lang. A computational algorithm for origami design. *Proceedings of the twelfth annual symposium on Computational geometry - SCG '96*, pages 98–105, 1996.

[20] Robert Lang and Thomas Hull. Origami design secrets: mathematical methods for an ancient art. *Springer*, 27:92–95, 2002.

[21] J. L. Silverberg, A.A. Evans, L. McLeod, R. C. Hayward, T. Hull, C. D. Santangelo, and I. Cohen. Using origami design principles to fold reprogrammable mechanical metamaterials. *Science*, 345(6197):647–650, aug 2014.

[22] Jesse L Silverberg, Jun-hee Na, Arthur a Evans, Bin Liu, Thomas C Hull, Christian D Santangelo, Robert J Lang, Ryan C Hayward, and Itai Cohen. Origami structures with a critical transition to bistability arising from hidden degrees of freedom. *Nature Materials*, (March):1–5, 2015.

[23] Shivendra Pandey, Margaret Ewing, Andrew Kunas, Nghi Nguyen, David H Gracias, and Govind Menon. Algorithmic design of self-folding polyhedra. *Proceedings of the National Academy of Sciences of the United States of America*, 108(50):19885–90, dec 2011.

[24] R. P. Feynman. There's plenty of room at the bottom. *Engineering and Science*, 23(5):22–36, 1960.

[25] H.C. Nathanson, W.E. Newell, R.A. Wickstrom, and Jr. Davis, J.R. The resonant gate transistor. *IEEE Transactions on Electron Devices*, 14(3):117–133, 1967.

[26] K.P. Rajurkar, G. Levy, a. Malshe, M.M. Sundaram, J. McGeough, X. Hu, R. Resnick, and a. DeSilva. Micro and Nano Machining by Electro-Physical and Chemical Processes. *CIRP Annals - Manufacturing Technology*, 55(2):643–666, 2006.

[27] S.M. Sze. *Semiconductor devices: physics and technology*. John Wiley & Sons, 2001.

[28] Vikas Choudhary and Krzysztof Iniewski. *MEMS: Fundamental Technology and Applications*. CRC Press, 2013.

[29] E Smela, O Inganäs, and I Lundström. Controlled folding of micrometer-size structures. *Science (New York, N.Y.)*, 268(5218):1735–8, jun 1995.

[30] Silas Alben, Bavani Balakrisnan, and Elisabeth Smela. Edge effects determine the direction of bilayer bending. *Nano letters*, 11(6):2280–5, jun 2011.

[31] E W Jager, E Smela, and O Inganäs. Microfabricating conjugated polymer actuators. *Science (New York, N.Y.)*, 290(5496):1540–5, nov 2000.

[32] Alexander Vorob'ev, Pablo Vaccaro, Kazuyoshi Kubota, Shanmugam Saravanan, and Tahito Aida. Array of Micromachined Components Fabricated Using Micro-Origami Method. *Japanese Journal of Applied Physics*, 42(Part 1, No. 6B):4024–4026, jun 2003.

[33] Scott T. Brittain, Olivier J. A. Schueller, Hongkai Wu, Sue Whitesides, and George M. Whitesides. Microorigami: Fabrication of Small, Three-Dimensional, Metallic Structures. *The Journal of Physical Chemistry B*, 105(2):347–350, jan 2001.

[34] Yingkai Liu, Lance Oh, S. Fanning, B. Shapiro, and E. Smela. Fabrication of folding microstructures actuated by polypyrrole/gold bilayer. In *TRANSDUCERS '03. 12th International Conference on Solid-State Sensors, Actuators and Microsystems. Digest of Technical Papers (Cat. No.03TH8664)*, volume 1, pages 786–789. IEEE, 2003.

[35] Kazuyoshi Kubota, Thomas Fleischmann, Shanmugam Saravanan, Pablo O. Vaccaro, and Tahito Aida. Self-Assembly of Microstage Using Micro-Origami Technique on GaAs. *Japanese Journal of Applied Physics*, 42(Part 1, No. 6B):4079–4083, jun 2003.

[36] Pablo O Vaccaro, K Kubota, T Fleischmann, S Saravanan, and T Aida. Valley-fold and mountain-fold in the micro-origami technique. *Microelectronics Journal*, 34(5-8):447–449, 2003.

[37] E.E. Hui, R.T. Howe, and M.S. Rodgers. Single-step assembly of complex 3-D microstructures. *Proceedings IEEE Thirteenth Annual International Conference on Micro Electro Mechanical Systems (Cat. No.00CH36308)*, m:602–607, 2000.

[38] Paul Stellman, Tilman Buchner, William J. Arora, and George Barbastathis. Dynamics of Nanostructured Origami. *Journal of Microelectromechanical Systems*, 16(4):932–949, 2007.

[39] Fabio Fachin, Stefan a. Nikles, and Brian L. Wardle. Mechanics of out-of-plane MEMS via Postbuckling: Model-experiment demonstration using CMOS. *Journal of Microelectromechanical Systems*, 21(3):621–634, 2012.

[40] Rohan Fernandes and David H Gracias. Self-folding polymeric containers for encapsulation and delivery of drugs. *Advanced drug delivery reviews*, 64(14):1579–89, nov 2012.

[41] Leonid Ionov. Bioinspired Microorigami by SelfFolding Polymer Films. *Macromolecular Chemistry and Physics*, pages 1178–1183, 2013.

[42] Charlotte Py, Paul Reverdy, Lionel Doppler, José Bico, Benoît Roman, and Charles N. Baroud. Capillary Origami: Spontaneous Wrapping of a Droplet with an Elastic Sheet. *Physical Review Letters*, 98(15):156103, apr 2007.

[43] Jeong-Hyun Cho, Teena James, and David H Gracias. Curving nanostructures using extrinsic stress. *Advanced materials (Deerfield Beach, Fla.)*, 22(21):2320–4, jun 2010.

[44] Evin Gultepe, Jatinder S. Randhawa, Sachin Kadam, Sumitaka Yamanaka, Florin M. Selaru, Eun J. Shin, Anthony N. Kalloo, and David H. Gracias. Biopsy with Thermally-Responsive Untethered Microtools. *Advanced Materials*, 25(4):514–519, jan 2013.

[45] Kate Malachowski, Mustapha Jamal, Qianru Jin, Beril Polat, Christopher J Morris, and David H Gracias. Self-Folding Single Cell Grippers. *Nano Letters*, 14(7):4164–4170, jul 2014.

[46] Jaehyun Park, Yevgeniy V. Kalinin, Sachin Kadam, Christina L. Randall, and David H. Gracias. Design for a Lithographically Patterned Bioartificial Endocrine Pancreas. *Artificial Organs*, 37(12):1059–1067, dec 2013.

[47] GG Stoney. The tension of metallic films deposited by electrolysis. *Proceedings of the Royal Society of London. Series A, ...*, 1909.

[48] S Timoshenko. Analysis of bi-metal thermostats. *J. Opt. Soc. Am*, 1925.

[49] J Y Ou, E Plum, L Jiang, and N I Zheludev. Reconfigurable photonic metamaterials. *Nano letters*, 11(5):2142–4, may 2011.

[50] John A Rogers, Takao Someya, and Yonggang Huang. Materials and mechanics for stretchable electronics. *Science (New York, N.Y.)*, 327(5973):1603–7, mar 2010.

[51] Georgi Stoychev, Svetlana Zakharchenko, Sébastien Turcaud, John W C Dunlop, and Leonid Ionov. Shape-programmed folding of stimuli-responsive polymer bilayers. *ACS nano*, 6(5):3925–34, may 2012.

[52] Srikanth Singamaneni, Michael E McConney, and Vladimir V Tsukruk. Swelling-induced folding in confined nanoscale responsive polymer gels. *ACS nano*, 4(4):2327–37, apr 2010.

[53] Georgi Stoychev, Nikolay Puretskiy, and Leonid Ionov. Self-folding all-polymer thermoresponsive microcapsules. *Soft Matter*, 7(7):3277, 2011.

[54] M. Huang, C. Boone, M. Roberts, D. E. Savage, M. G. Lagally, N. Shaji, H. Qin, R. Blick, J. a. Nairn, and F. Liu. Nanomechanical Architecture of Strained Bilayer Thin Films: From Design Principles to Experimental Fabrication. *Advanced Materials*, 17(23):2860–2864, dec 2005.

[55] Mustapha Jamal, Aasiyeh M Zarafshar, and David H Gracias. Differentially photo-crosslinked polymers enable self-assembling microfluidics. *Nature communications*, 2:527, jan 2011.

[56] Troy R Hendricks and Iisoon Lee. Wrinkle-free nanomechanical film: Control and prevention of polymer film buckling. *Nano Letters*, 7(2):372–379, 2007.

[57] E Hawkes, B An, N M Benbernou, H Tanaka, S Kim, E D Demaine, D Rus, and R J Wood. Programmable matter by folding. *Proceedings of the National Academy of Sciences of the United States of America*, 107(28):12441–5, jul 2010.

[58] Jamie K Paik, Elliot Hawkes, and Robert J Wood. A novel low-profile shape memory alloy torsional actuator. *Smart Materials and Structures*, 19:125014, 2010.

[59] Samuel M. Felton, Michael T. Tolley, ByungHyun Shin, Cagdas D. Onal, Erik D. Demaine, Daniela Rus, and Robert J. Wood. Self-folding with shape memory composites. *Soft Matter*, 9(32):7688, 2013.

[60] Z. Tang, Y. Wang, P. Podsiadlo, and N.a. Kotov. Biomedical Applications of Layer-by-Layer Assembly: From Biomimetics to Tissue Engineering. *Advanced Materials*, 18(24):3203–3224, dec 2006.

[61] Xiaobo Zhang, Cary L Pint, Min Hyung Lee, Bryan Edward Schubert, Arash Jamshidi, Kuniharu Takei, Hyunhyub Ko, Andrew Gillies, Rizia Bardhan, Jeffrey J Urban, Ming Wu, Ronald Fearing, and Ali Javey. Optically- and thermally-responsive programmable materials based on carbon nanotube-hydrogel polymer composites. *Nano letters*, 11(8):3239–44, aug 2011.

[62] Shoji Takeuchi, Takafumi Suzuki, Kunihiko Mabuchi, and Hiroyuki Fujita. 3D flexible multichannel neural probe array. *Journal of Micromechanics and Microengineering*, 14:104–107, 2004.

[63] Ying Yao, Mayurachat Ning Gulari, James a. Wiler, and Kensall D. Wise. A microassembled low-profile three-dimensional microelectrode array for neural prosthesis applications. *Journal of Microelectromechanical Systems*, 16(4):977–988, 2007.

[64] Nadrian C. Seeman. Nucleic acid junctions and lattices. *Journal of Theoretical Biology*, 99(2):237–247, nov 1982.

[65] Paul W K Rothemund. Folding DNA to create nanoscale shapes and patterns. *Nature*, 440(7082):297–302, mar 2006.

[66] Akinori Kuzuya and Makoto Komiyama. Design and construction of a box-shaped 3D-DNA origami. *Chemical Communications*, (28):4182, 2009.

[67] Robert Schreiber, Susanne Kempter, Stefan Holler, Verena Schüller, Daniel Schiffels, Stephanie S Simmel, Philipp C Nickels, and Tim Liedl. DNA Origami-Templated Growth of Arbitrarily Shaped Metal Nanoparticles. *Small*, 7(13):1795–1799, jul 2011.

[68] Robert Schreiber, Jaekwon Do, Eva-maria Roller, Tao Zhang, Verena J Schüller, Philipp C Nickels, Jochen Feldmann, and Tim Liedl. Hierarchical assembly of metal nanoparticles, quantum dots and organic dyes using DNA origami scaffolds. *Nature Nanotechnology*, 9(1):74–78, dec 2013.

[69] D Han, S Pal, J Nangreave, Z Deng, Y Liu, and H Yan. DNA Origami with Complex Curvatures in Three-Dimensional Space. *Science*, 332:342–347, 2011.

[70] William M Shih and Chenxiang Lin. Knitting complex weaves with DNA origami. *Current Opinion in Structural Biology*, 20(3):276–282, 2010.

[71] Dongran Han, Suchetan Pal, Yan Liu, and Hao Yan. Folding and cutting DNA into reconfigurable topological nanostructures. *Nature nanotechnology*, 5(10):712–7, oct 2010.

[72] Melina K. Blees, Arthur W. Barnard, Peter A. Rose, Samantha P. Roberts, Kathryn L. McGill, Pinshane Y. Huang, Alexander R. Ruyack, Joshua W. Kevek, Bryce Kobrin, David a. Muller, and Paul L. McEuen. Graphene kirigami. *Nature*, 2015.

[73] Shuze Zhu and Teng Li. Hydrogenation-Assisted Graphene Origami and Its Application in Programmable Molecular Mass Uptake, Storage, and Release. *ACS Nano*, 8(3):2864–2872, mar 2014.

[74] Paul Zakharia Fajar Hanakata, Zenan Qi, David Campbell, and Harold Park. Highly Stretchable MoS2 Kirigami. *Nanoscale*, V, 2015.

[75] Oleg V. Yazyev and Yong P. Chen. Polycrystalline graphene and other two-dimensional materials. *Nature Nanotechnology*, 9(10):755–767, 2014.

[76] Steven P. Koenig, Narasimha G. Boddeti, Martin L. Dunn, and J. Scott Bunch. Ultrastrong adhesion of graphene membranes. *Nature Nanotechnology*, 6(9):543–546, 2011.

[77] Raquel Verdejo, M. Mar Bernal, Laura J. Romasanta, and Miguel a. Lopez-Manchado. Graphene filled polymer nanocomposites. *Journal of Materials Chemistry*, 21:3301, 2011.

[78] Jian Zhu, Huanan Zhang, and Nicholas A. Kotov. Thermodynamic and structural insights into nanocomposites engineering by comparing two materials assembly techniques for graphene. *ACS Nano*, 7(6):4818–4829, 2013.

[79] Peng Zhang, Lulu Ma, Feifei Fan, Zhi Zeng, Cheng Peng, Phillip E. Loya, Zheng Liu, Yongji Gong, Jiangnan Zhang, Xingxiang Zhang, Pulickel M. Ajayan, Ting Zhu, and Jun Lou. Fracture toughness of graphene. *Nature Communications*, 5:1–7, 2014.

[80] Zenan Qi, Harold S. Park, and David K. Campbell. Highly Deformable Graphene Kirigami. page 5, jul 2014.

[81] Peter Fratzl and Richard Weinkamer. Natures hierarchical materials. *Progress in Materials Science*, 52(8):1263–1334, nov 2007.

[82] MA Meyers, J McKittrick, and PY Chen. Structural biological materials: critical mechanics-materials connections. *Science*, (February):773–779, 2013.

[83] Ray F Egerton. *Physical principles of electron microscopy*. Springer Science, 2005.

[84] M Minsky. Microscopy Apparatus. *US Patent 3013467*, 3013467:5, 1961.

[85] Nathan S Claxton, Thomas J Fellers, and Michael W Davidson. Laser Scanning Confocal Microscopy. *Encyclopedia of Medical Devices and Instrumentation*, 1979(21):1–37, 2006.

[86] Wojciech Kaplonek and Krzysztof Nadolny. Advanced 3D laser microscopy for measurements and analysis of vitrified bonded abrasive tools. *Journal of Engineering Science and Technology*, 7(6):661–678, 2012.

[87] L.R.G. Treloar. *Physics of Rubber Elasticity*. Oxford University Press, UK, 2005.

[88] C Storm, J. J. Pastore, F. C. MacKintosh, T. C. Lubensky, and P. A. Janmey. Nonlinear elasticity in biological gels. *Nature*, 435(May):0–3, 2005.

[89] Prashant K Purohit, Rustem I Litvinov, Andre E X Brown, Dennis E Discher, and John W Weisel. Protein unfolding accounts for the unusual mechanical behavior of fibrin networks. *Acta biomaterialia*, 7(6):2374–83, jun 2011.

[90] Mary C. Boyce and Ellen M. Arruda. Constitutive Models of Rubber Elasticity: A Review. *Rubber Chemistry and Technology*, 73(3):504–523, jul 2000.

[91] John Gosline, Margo Lillie, Emily Carrington, Paul Guerette, Christine Ortlepp, and Ken Savage. Elastic proteins: biological roles and mechanical properties. *Philosophical transactions of the Royal Society of London. Series B, Biological sciences*, 357(1418):121–32, feb 2002.

[92] Steven W Cranford, Anna Tarakanova, Nicola M Pugno, and Markus J Buehler. Nonlinear material behaviour of spider silk yields robust webs. *Nature*, 482(7383):72–6, feb 2012.

[93] MF Ashby and RFM Medalist. The mechanical properties of cellular solids. *Metallurgical Transactions A*, 14(September):1755–1769, 1983.

[94] J. Bauer, S. Hengsbach, I. Tesari, R. Schwaiger, and O. Kraft. High-strength cellular ceramic composites with 3D microarchitecture. *Proceedings of the National Academy of Sciences*, pages 1–6, feb 2014.

[95] Douglas T. Queheillalt and Haydn N.G. Wadley. Cellular metal lattices with hollow trusses. *Acta Materialia*, 53(2):303–313, jan 2005.

[96] Lorna J. Gibson and Michael F. Ashby. *Cellular solids: structure and properties*. Cambridge University Press, Cambridge, U.K., 2nd edition, 1999.

[97] W Johnson. *Impact Strength of Materials*. Edward Arnold, 1972.

[98] Oliver Buhler. *A Brief Introduction to Classical, Statistical, and Quantum Mechanics*. American Mathematical Society and the Courant Institue of Mathmatical Sciences at New York University., New York, 2006.

[99] S.D. Papka and S. Kyriakides. In-plane biaxial crushing of honeycombsPart II Analysis, 1999.

[100] N. Ohno, D. Okumura, and T. Niikawa. Long-wave buckling of elastic square honeycombs subject to in-plane biaxial compression. *International Journal of Mechanical Sciences*, 46:1697–1713, 2004.

[101] T. Mullin, S. Deschanel, K. Bertoldi, and M. Boyce. Pattern Transformation Triggered by Deformation. *Physical Review Letters*, 99(8):1–4, aug 2007.

[102] Zhiyong Tang, Nicholas A. Kotov, Sergei Magonov, and Birol Ozturk. Nanostructured artificial nacre. *Nature Materials*, 2(6):413–8, jun 2003.

[103] Ming Yang, Ying Hou, and Nicholas a. Kotov. Graphene-based multilayers: Critical evaluation of materials assembly techniques. *Nano Today*, 7:430–447, 2012.

[104] Nobuyuki Sakai, Takayoshi Sasaki, Kazuki Matsubara, and Tetsu Tatsuma. Layer-by-layer assembly of gold nanoparticles with titania nanosheets: control of plasmon resonance and photovoltaic properties. *Journal of Materials Chemistry*, 20(21):4371, 2010.

[105] Praveen Sher, Catarina a Custódio, and João F Mano. Layer-by-layer technique for producing porous nanostructured 3D constructs using moldable freeform assembly of spherical templates. *Small (Weinheim an der Bergstrasse, Germany)*, 6(23):2644–8, dec 2010.

[106] Paul Podsiadlo, Stephen Paternel, Jean-Marie Rouillard, Zhengfei Zhang, Jaebeom Lee, Jung-Woo Lee, Erdogan Gulari, and Nicholas a Kotov. Layer-by-layer assembly of nacre-like nanostructured composites with antimicrobial properties. *Langmuir : the ACS journal of surfaces and colloids*, 21(25):11915–21, dec 2005.

[107] Sudhanshu Srivastava and Nicholas a Kotov. Composite Layer-by-Layer (LBL) assembly with inorganic nanoparticles and nanowires. *Accounts of chemical research*, 41(12):1831–41, dec 2008.

[108] NanoStrata Inc. nanoStrata Inc.

[109] C. Jiang and V.V. Tsukruk. Freestanding Nanostructures via Layer-by-Layer Assembly. *Advanced Materials*, 18(7):829–840, apr 2006.

[110] Y.-H. Lin, C. Jiang, J. Xu, Z. Lin, and V. V. Tsukruk. Sculptured Layer-by-Layer Films. *Advanced Materials*, 19(22):3827–3832, nov 2007.

[111] Yoonseob Kim, Jian Zhu, Bongjun Yeom, Matthew Di Prima, Xianli Su, Jin-Gyu Kim, Seung Jo Yoo, Ctirad Uher, and Nicholas A Kotov. Stretchable nanoparticle conductors with self-organized conductive pathways. *Nature*, 500(7460):59–63, aug 2013.

[112] J Bühler, F-P Steiner, and H Baltes. Silicon dioxide sacrificial layer etching in surface micromachining. *Journal of Micromechanics and Microengineering*, 7:R1–R13, 1999.

[113] E Bassous and E.F. Baran. The Fabrication of High Precision Nozzles by the Anisotropic Etching of (100) Silicon. *Journal of The Electrochemical Society*, 125(8):1321, 1978.

[114] Kevin M McPeak, Christian D van Engers, Mark Blome, Jong Hyuk Park, Sven Burger, Miguel a Gosálvez, Ava Faridi, Yasmina R Ries, Ayaskanta Sahu, and David J Norris. Complex chiral colloids and surfaces via high-index off-cut silicon. *Nano letters*, 14(5):2934–40, may 2014.

[115] R. G. Poulsen. Plasma etching in integrated circuit manufacture: A review. *Journal of Vacuum Science and Technology*, 14(1):266, jan 1977.

[116] B.-J. de Gans, P. C. Duineveld, and U. S. Schubert. Inkjet Printing of Polymers: State of the Art and Future Developments. *Advanced Materials*, 16(3):203–213, feb 2004.

[117] Madhusudan Singh, Hanna M. Haverinen, Parul Dhagat, and Ghassan E. Jabbour. Inkjet Printing-Process and Its Applications. *Advanced Materials*, 22(6):673–685, feb 2010.

[118] Herman Wijshoff. The dynamics of the piezo inkjet printhead operation. *Physics Reports*, 491(4-5):77–177, 2010.

[119] Lord Rayleigh. On the Instability of Jets. *Proceedings of London Mathematical Society*, 10(June 1873):4–13, 1878.

[120] Dimatix. Jettable Fluid Formulation Guidelines. Technical report, FUJIFILM Dimatix Inc, Santa Clara, CA, 2013.

[121] J. A. Lewis. Direct Ink Writing of 3D Functional Materials. *Advanced Functional Materials*, 16(17):2193–2204, nov 2006.

[122] Bok Yeop Ahn, Daisuke Shoji, Christopher J Hansen, Eunji Hong, David C Dunand, and Jennifer A Lewis. Printed Origami Structures. *Advanced Materials*, 22(20):2251–2254, may 2010.

[123] Christine M Andres and Nicholas A Kotov. Inkjet deposition of layer-by-layer assembled films. *Journal of the American Chemical Society*, 132(41):14496–502, oct 2010.

[124] Rattanon Suntivich, Olga Shchepelina, Ikjun Choi, and Vladimir V. Tsukruk. Inkjet-assisted layer-by-layer printing of encapsulated arrays. *ACS Applied Materials and Interfaces*, 4:3102–3110, 2012.

[125] Bahador Farshchian, Sooyeon Park, Junseo Choi, Alborz Amirsadeghi, Jaejong Lee, and Sunggook Park. 3D nanomolding for lab-on-a-chip applications. *Lab on a chip*, 12(22):4764–71, nov 2012.

[126] Matthew E Stewart, Christopher R Anderton, Lucas B Thompson, Joana Maria, Stephen K Gray, John a Rogers, and Ralph G Nuzzo. Nanostructured plasmonic sensors. *Chemical reviews*, 108(2):494–521, feb 2008.

[127] T. L. Breen. Design and Self-Assembly of Open, Regular, 3D Mesostructures. *Science*, 284(May):948–951, 1999.

[128] Y. Zhang, S. Wang, M. Eghtedari, M. Motamedi, and N. a. Kotov. Inverted-Colloidal-Crystal Hydrogel Matrices as Three-Dimensional Cell Scaffolds. *Advanced Functional Materials*, 15(5):725–731, may 2005.

[129] C B Murray, C R Kagan, and M G Bawendi. Self-Organization of Cdse Nanocrystallites into 3-Dimensional Quantum-Dot Superlattices. *Science*, 270(5240):1335–1338, 1995.

[130] J. W. van Honschoten, J. W. Berenschot, T. Ondarcuhu, R. G. P. Sanders, J. Sundaram, M. Elwenspoek, and N. R. Tas. Elastocapillary fabrication of three-dimensional microstructures. *Applied Physics Letters*, 97(1):014103, 2010.

[131] Jun-Hee Na, Arthur A Evans, Jinhye Bae, Maria C Chiappelli, Christian D Santangelo, Robert J Lang, Thomas C Hull, and Ryan C Hayward. Programming Reversibly Self-Folding Origami with Micropatterned Photo-Crosslinkable Polymer Trilayers. *Advanced materials (Deerfield Beach, Fla.)*, pages 79–85, oct 2014.

[132] Jennie Ryu, Matteo DAmato, Xiaodong Cui, Kevin N. Long, H. Jerry Qi, and Martin L. Dunn. Photo-origamiBending and folding polymers with light. *Applied Physics Letters*, 100(16):161908, 2012.

[133] Ying Liu, Julie K. Boyles, Jan Genzer, and Michael D. Dickey. Self-folding of polymer sheets using local light absorption. *Soft Matter*, 8(6):1764, 2012.

[134] Ren Geryak and Vladimir V Tsukruk. Reconfigurable and actuating structures from soft materials. *Soft matter*, 10(9):1246–63, 2014.

[135] William J. Arora, Anthony J. Nichol, Henry I. Smith, and George Barbastathis. Membrane folding to achieve three-dimensional nanostructures: Nanopatterned silicon nitride folded with stressed chromium hinges. *Applied Physics Letters*, 88(5):053108, 2006.

[136] Noy Bassik, George M Stern, and David H Gracias. Microassembly based on hands free origami with bidirectional curvature. *Applied physics letters*, 95(9):91901, aug 2009.

[137] Jeong-Hyun Cho, Michael D Keung, Niels Verellen, Liesbet Lagae, Victor V Moshchalkov, Pol Van Dorpe, and David H Gracias. Nanoscale origami for 3D optics. *Small (Weinheim an der Bergstrasse, Germany)*, 7(14):1943–8, jul 2011.

[138] Sung Yun Yang and Michael F Rubner. Micropatterning of polymer thin films with pH-sensitive and cross-linkable hydrogen-bonded polyelectrolyte multilayers. *Journal of the American Chemical Society*, 124(10):2100–2101, 2002.

[139] Nicholas A. Kotov. Ordered Layered Assemblies of Nanoparticles. *MRS Bulletin*, 26(12):992–997, dec 2001.

[140] Christine M Andres, Jian Zhu, Terry Shyu, Connor Flynn, and Nicholas A Kotov. Shape-morphing nanocomposite origami. *Langmuir : the ACS journal of surfaces and colloids*, 30(19):5378–85, may 2014.

[141] Shaoqin Liu, Dirk G Kurth, and Dirk Volkmer. Polyoxometalates as pH-sensitive probes in self-assembled multilayers. *Chemical communications (Cambridge, England)*, 10(9):976–7, may 2002.

[142] Ralf Köhler, Ingo Dönch, Patrick Ott, André Laschewsky, Andreas Fery, and Rumen Krastev. Neutron reflectometry study of swelling of polyelectrolyte multilayers in water vapors: influence of charge density of the polycation. *Langmuir : the ACS journal of surfaces and colloids*, 25(19):11576–85, oct 2009.

[143] C Gao, E Donath, S Moya, V. Dudnik, and H. Möhwald. Elasticity of hollow polyelectrolyte capsules prepared by the layer-by-layer technique. *European Physical Journal E*, 5(1):21–27, 2001.

[144] Paul Podsiadlo, Marc Michel, Kevin Critchley, Sudhanshu Srivastava, Ming Qin, Jung Woo Lee, Eric Verploegen, A. John Hart, Ying Qi, and Nicholas A. Kotov. Diffusional Self-Organization in Exponential Layer-By-Layer Films with Micro- and Nanoscale Periodicity. *Angewandte Chemie International Edition*, 48(38):7073–7077, 2009.

[145] Jian Zhu, Christine M Andres, Jiadi Xu, Ayyalusamy Ramamoorthy, Thomas Tsotsis, and Nicholas a Kotov. Pseudonegative thermal expansion and the state of water in graphene oxide layered assemblies. *ACS Nano*, 6(9):8357–65, oct 2012.

[146] Aurélie Lafuma and David Quéré. Superhydrophobic states. *Nature Materials*, 2(7):457–60, jul 2003.

[147] Jau-ye Shiu, Chun-wen Kuo, Peilin Chen, and Chung-Yuan Mou. Fabrication of Tunable Superhydrophobic Surfaces by Nanosphere Lithography. *Chemistry of Materials*, 16(4):561–564, feb 2004.

[148] David Quéré. Wetting and Roughness. *Annual Review of Materials Research*, 38(1):71–99, aug 2008.

[149] Eero Huovinen, Laura Takkunen, Tarmo Korpela, Mika Suvanto, Tuula T. Pakkanen, and Tapani a. Pakkanen. Mechanically robust superhydrophobic polymer surfaces based on protective micropillars. *Langmuir*, 30(5):1435–1443, 2014.

[150] Lie Shen, Wenlian Qiu, Bin Liu, and Qipeng Guo. Stable superhydrophobic surface based on silicone combustion product. *RSC Adv.*, 4(99):56259–56262, 2014.

[151] D. Oner and T. J. McCarthy. Ultra-Hydrophobic Surfaces:Effects of Topography Length Scales on Wettability. *Langmuir*, 16(2):7777–7782, 2000.

[152] Kyoung G Lee, Bong Gill Choi, Byeong Il Kim, Terry Shyu, Myung Seok Oh, Sung Gap Im, Sung-Jin Chang, Tae Jae Lee, Nicholas A. Kotov, and Seok Jae

Lee. Scalable nanopillar arrays with layer-by-layer patterned overt and covert images. *Advanced materials (Deerfield Beach, Fla.)*, 26(35):6119–24, sep 2014.

[153] Alexandra Schweikart and Andreas Fery. Controlled wrinkling as a novel method for the fabrication of patterned surfaces. *Microchimica Acta*, 165(3-4):249–263, apr 2009.

[154] Sung H. Kang, Boaz Pokroy, L. Mahadevan, and Joanna Aizenberg. Control of shape and size of nanopillar assembly by adhesion-mediated elastocapillary interaction. *ACS Nano*, 4(11):6323–6331, 2010.

[155] AK Geim, S V Dubonos, I V Grigorieva, K S Novoselov, a a Zhukov, and S Yu Shapoval. Microfabricated adhesive mimicking gecko foot-hair. *Nature materials*, 2:461–463, 2003.

[156] Ren Zhu, Wengui Zhang, Chao Li, and Rusen Yang. Uniform zinc oxide nanowire arrays grown on nonepitaxial surface with general orientation control. *Nano letters*, 13(11):5171–6, nov 2013.

[157] Y N Xia, P D Yang, Y G Sun, Y Y Wu, B Mayers, B Gates, Y D Yin, F Kim, and Y Q Yan. One-dimensional nanostructures: Synthesis, characterization, and applications. *Advanced Materials*, 15(5):353–389, 2003.

[158] Bernhard Wolfrum, Yulia Mourzina, Dirk Mayer, Daniel Schwaab, and Andreas Offenhäusser. Fabrication of large-scale patterned gold-nanopillar arrays on a silicon substrate using imprinted porous alumina templates. *Small*, 2(11):1256–1260, 2006.

[159] C F Huang, Y Lin, Y K Shen, and Y M Fan. Optimal processing for hydrophobic nanopillar polymer surfaces using nanoporous alumina template. *Applied Surface Science*, 305(0):419–426, 2014.

[160] Anish Tuteja, Wonjae Choi, Minglin Ma, Joseph M Mabry, Sarah a Mazzella, Gregory C Rutledge, Gareth H McKinley, and Robert E Cohen. Designing superoleophobic surfaces. *Science (New York, N.Y.)*, 318(5856):1618–22, dec 2007.

[161] Sai P R Kobaku, Arun K. Kota, Duck Hyun Lee, Joseph M. Mabry, and Anish Tuteja. Patterned superomniphobic-superomniphilic surfaces: Templates for site-selective self-assembly. *Angewandte Chemie - International Edition*, 51(2):10109–10113, 2012.

[162] Tsuyoshi Sekitani, Yoshiaki Noguchi, Kenji Hata, Takanori Fukushima, Takuzo Aida, and Takao Someya. A rubberlike stretchable active matrix using elastic conductors. *Science (New York, N.Y.)*, 321(5895):1468–72, sep 2008.

[163] J Song, H Jiang, Z Liu, D Khang, Y Huang, J Rogers, C Lu, and C Koh. Buckling of a stiff thin film on a compliant substrate in large deformation. *International Journal of Solids and Structures*, 45(10):3107–3121, may 2008.

[164] Dahl-Young Khang, Jianliang Xiao, Coskun Kocabas, Scott MacLaren, Tony Banks, Hanqing Jiang, Yonggang Y Huang, and John A Rogers. Molecular scale buckling mechanics in individual aligned single-wall carbon nanotubes on elastomeric substrates. *Nano letters*, 8(1):124–30, jan 2008.

[165] Jonathan A Fan, Woon-Hong Yeo, Yewang Su, Yoshiaki Hattori, Woosik Lee, Sung-Young Jung, Yihui Zhang, Zhuangjian Liu, Huanyu Cheng, Leo Falgout, Mike Bajema, Todd Coleman, Dan Gregoire, Ryan J Larsen, Yonggang Huang, and John A Rogers. Fractal design concepts for stretchable electronics. *Nature communications*, 5:3266, jan 2014.

[166] M. Mirkhalaf, A. Khayer Dastjerdi, and F. Barthelat. Overcoming the brittleness of glass through bio-inspiration and micro-architecture. *Nature communications*, 5:3166, jan 2014.

[167] Ahmad Khayer Dastjerdi, Reza Rabiei, and Francois Barthelat. The weak interfaces within tough natural composites: experiments on three types of nacre. *Journal of the mechanical behavior of biomedical materials*, 19:50–60, mar 2013.

[168] Ying Zhang, Elisabetta a Matsumoto, Anna Peter, Pei-Chun Lin, Randall D Kamien, and Shu Yang. One-Step Nanoscale Assembly of Complex Structures via Harnessing of an Elastic Instability. *Nano letters*, 8(4):1192–6, apr 2008.

[169] D. P. Holmes and A. J. Crosby. Snapping Surfaces. *Advanced Materials*, 19(21):3589–3593, nov 2007.

[170] Srikanth Singamaneni, Katia Bertoldi, Sehoon Chang, Ji-Hyun Jang, Edwin L Thomas, Mary C Boyce, and Vladimir V Tsukruk. Instabilities and pattern transformation in periodic, porous elastoplastic solid coatings. *ACS applied materials & interfaces*, 1(1):42–7, jan 2009.

[171] Sung Hoon Kang, Sicong Shan, Wim L Noorduin, Mughees Khan, Joanna Aizenberg, and Katia Bertoldi. Buckling-Induced Reversible Symmetry Breaking and Amplification of Chirality Using Supported Cellular Structures. *Advanced materials (Deerfield Beach, Fla.)*, pages 3380–3385, may 2013.

[172] Chuan Fei Guo, Tianyi Sun, Qihan Liu, Zhigang Suo, and Zhifeng Ren. Highly stretchable and transparent nanomesh electrodes made by grain boundary lithography. *Nature communications*, 5:3121, 2014.

[173] Terry C. Shyu, Pablo F. Damasceno, Paul M. Dodd, Aaron Lamoureux, Lizhi Xu, Matthew Shlian, Max Shtein, Sharon C. Glotzer, and Nicholas A. Kotov. A kirigami approach to engineering elasticity in nanocomposites through patterned defects. *Nature Materials*, 14(August):785–790, 2015.

[174] Aaron Lamoureux, Kyusang Lee, Matthew Shlian, Stephen R. Forrest, and Max Shtein. Dynamic kirigami structures for integrated solar tracking. *Nature Communications*, 6:8092, 2015.

[175] Bong Sup Shim, Jian Zhu, Edward Jan, Kevin Critchley, Szushen Ho, Paul Podsiadlo, Kai Sun, and Nicholas a Kotov. Multiparameter Structural Optimization of Single-Walled Carbon Nanotube Stiffness , and Toughness. *ACS Nano*, 3(7):1711–1722, 2009.

[176] F.W. Peek. *Dielectric Phenomena in High-Voltage Engineering.* McGraw-Hill, New York, 3 edition, 1929.

[177] Yihui Zhang, Zheng Yan, Kewang Nan, Dongqing Xiao, Yuhao Liu, Haiwen Luan, Haoran Fu, Xizhu Wang, Qinglin Yang, Jiechen Wang, Wen Ren, Hongzhi Si, Fei Liu, Lihen Yang, Hejun Li, Juntong Wang, Xuelin Guo, Hongying Luo, Liang Wang, Yonggang Huang, and John A. Rogers. A mechanically driven form of Kirigami as a route to 3D mesostructures in micro/nanomembranes. *Proceedings of the National Academy of Sciences*, 112(38):201515602, 2015.

[178] Lewi Tonks and Irving Langmuir. Oscillations in ionized gases. *Physical Review*, 33(2):195–210, 1929.

[179] Riccardo D'Agostino, Pietro Favia, Christian Oehr, and Michael R. Wertheimer. Low-Temperature Plasma Processing of Materials: Past, Present, and Future. *Plasma Processes and Polymers*, 2(1):7–15, 2005.

[180] James W Gregory, C Lon Enloe, Gabriel I Font, and Thomas E McLaughlin. Force Production Mechanism of a Dielectric-Barrier Discharge Plasma Actuator. *Aiaa 2007-185*, (January):1–13, 2007.

[181] Kunwar Pal Singh and Subrata Roy. Physics of plasma actuator operating in atmospheric air. *Applied Physics Letters*, 92(2008):11–13, 2008.

[182] Rasool Erfani, Hossein Zare-Behtash, Craig Hale, and Konstantinos Kontis. Development of DBD plasma actuators: The double encapsulated electrode. *Acta Astronautica*, 109:132–143, 2015.

[183] U. Schlickum, R. Decker, F. Klappenberger, G. Zoppellaro, S. Klyatskaya, W. Auwärter, S. Neppl, K. Kern, H. Brune, M. Ruben, and J. V. Barth. Chiral kagomé lattice from simple ditopic molecular bricks. *Journal of the American Chemical Society*, 130(35):11778–11782, 2008.

[184] J. N. Grima and K. E. Evans. Auxetic behavior from rotating squares. *Journal of Materials Science Letters*, 19(17):1563–1565, 2000.

[185] Rivka Elbaum, Liron Zaltzman, Ingo Burgert, and Peter Fratzl. The role of wheat awns in the seed dispersal unit. *Science (New York, N.Y.)*, 316(5826):884–6, may 2007.

[186] Matthew J Harrington, Khashayar Razghandi, Friedrich Ditsch, Lorenzo Guiducci, Markus Rueggeberg, John W C Dunlop, Peter Fratzl, Christoph Neinhuis, and Ingo Burgert. Origami-like unfolding of hydro-actuated ice plant seed capsules. *Nature communications*, 2(May):337, jan 2011.

[187] John W C Dunlop, Richard Weinkamer, and Peter Fratzl. Artful interfaces within biological materials. *Materials Today*, 14(3):70–78, 2011.

[188] Srikanth Singamaneni, Katia Bertoldi, Sehoon Chang, Ji-Hyun Jang, Seth L. Young, Edwin L. Thomas, Mary C. Boyce, and Vladimir V. Tsukruk. Bifurcated Mechanical Behavior of Deformed Periodic Porous Solids. *Advanced Functional Materials*, 19(9):1426–1436, may 2009.

[189] Jongmin Shim, Claude Perdigou, Elizabeth Chen, Katia Bertoldi, and Pedro M Reis. Buckling-induced encapsulation of structured elastic shells under pressure. *Proceedings of the National Academy of Sciences of the United States of America*, 109(16):5978–5983, 2012.

[190] Jatinder S. Randhawa, Kate E. Laflin, Natasha Seelam, and David H. Gracias. Microchemomechanical Systems. *Advanced Functional Materials*, 21(13):2395–2410, jul 2011.

[191] Yihui Zhang, Sheng Xu, Haoran Fu, Juhwan Lee, Jessica Su, Keh-Chih Hwang, John A. Rogers, and Yonggang Huang. Buckling in serpentine microstructures and applications in elastomer-supported ultra-stretchable electronics with high areal coverage. *Soft Matter*, 9(33):8062, 2013.

[192] Bavani Balakrisnan, Aleksandar Nacev, Jeffrey M Burke, Abhijit Dasgupta, and Elisabeth Smela. Design of compliant meanders for applications in MEMS, actuators, and flexible electronics. *Smart Materials and Structures*, 21(7):075033, jul 2012.

[193] T. A. Schaedler, A. J. Jacobsen, A. Torrents, A. E. Sorensen, J. Lian, J. R. Greer, L. Valdevit, and W. B. Carter. Ultralight Metallic Microlattices. *Science*, 334(6058):962–965, 2011.

[194] Xiaoyu Zheng, Howon Lee, Todd H Weisgraber, Maxim Shusteff, Joshua DeOtte, Eric B Duoss, Joshua D Kuntz, Monika M Biener, Qi Ge, Julie a Jackson, Sergei O Kucheyev, Nicholas X Fang, and Christopher M Spadaccini. Ultralight, ultrastiff mechanical metamaterials. *Science (New York, N.Y.)*, 344(6190):1373–7, jun 2014.

[195] Lucas R Meza, Satyajit Das, and Julia R Greer. Strong, lightweight, and recoverable three-dimensional ceramic nanolattices. *Science*, 345(6202):1322–1326, sep 2014.

[196] Lauren C. Montemayor, Lucas R. Meza, and Julia R. Greer. Design and fabrication of hollow rigid nanolattices via two-photon lithography. *Advanced Engineering Materials*, 16(2):184–189, 2014.

[197] Dongchan Jang, Lucas R Meza, Frank Greer, and Julia R Greer. Fabrication and deformation of three-dimensional hollow ceramic nanostructures. *Nature materials*, 12(10):893–898, sep 2013.